
SamGoG: A Sampling-Based Graph-of-Graphs Framework for Imbalanced Graph Classification

Shangyou Wang^{1,3,†}, Zezhong Ding^{1,3,†}, Xike Xie^{2,3*}

¹School of Artificial Intelligence and Data Science, University of Science and Technology of China (USTC)

²School of Biomedical Engineering, USTC

³Data Darkness Lab, Suzhou Institute for Advanced Research, USTC

{wash_you, zezhongding}@mail.ustc.edu.cn, xkxie@ustc.edu.cn

Abstract

Graph Neural Networks (GNNs) have shown remarkable success in graph classification tasks by capturing both structural and feature-based representations. However, real-world graphs often exhibit two critical forms of imbalance: class imbalance and graph size imbalance. These imbalances can bias the learning process and degrade model performance. Existing methods typically address only one type of imbalance or incur high computational costs. In this work, we propose SamGoG, a **sampling-based Graph-of-Graphs (GoG)** learning framework that effectively mitigates both class and graph size imbalance. SamGoG constructs multiple GoGs through an efficient importance-based sampling mechanism and trains on them sequentially. This sampling mechanism incorporates the learnable pairwise similarity and adaptive GoG node degree to enhance edge homophily, thus improving downstream model quality. SamGoG can seamlessly integrate with various downstream GNNs, enabling their efficient adaptation for graph classification tasks. Extensive experiments on benchmark datasets demonstrate that SamGoG achieves state-of-the-art performance with up to a **15.66%** accuracy improvement with **6.7×** training acceleration.

1 Introduction

Graph classification is a supervised learning task that seeks to learn a predictive function $f : g \rightarrow \mathcal{C}$ on a set of graphs $\mathbb{G} = \{g_i\}_{i=1}^N$, utilizing a labeled subset $\mathbb{G}_L = \{g_i\}_{i=1}^{N_L} \subset \mathbb{G}$. Each graph $g_i \in \mathbb{G}_L$ is represented as $g_i = (A_i, X_i, y_i)$, where A_i is the corresponding adjacent matrix, X_i is the node feature matrix, and $y_i \in \mathcal{C}$ is the class label, with \mathcal{C} being the set of possible classes. The goal is to learn a function f that generalizes to predict labels for unlabeled graphs in $\mathbb{G}_U = \mathbb{G} \setminus \mathbb{G}_L$, by leveraging their structures and features. This task has wide-ranging applications in areas such as social network analysis [1] and bioinformatics [2, 3], facilitating tasks like community detection, molecular property prediction, and protein function analysis. To this end, GNNs [4, 5] have become the leading method due to their ability to jointly model graph structural information and node features.

Despite the success of GNNs, graph classification under imbalanced conditions remains a significant challenge, primarily due to two common issues: **class imbalance**, where some classes contain far more training graphs than others [6, 7] (see Figure 1(a)), and **graph size imbalance**, where input graphs vary substantially in size (i.e., number of nodes) [8, 9] (see Figure 1(b)). Class imbalance biases models toward majority classes, degrading the performance of minority ones, while graph size imbalance impairs performance on small graphs and hinders generalization under distribution shifts. Existing methods fall into data-centric (e.g., class resampling, synthetic augmentation) [10, 11, 12, 13] and algorithmic-centric (e.g., subgraph matching, pattern extraction) [9, 14, 8] categories, but both face computational bottlenecks and limited effectiveness in handling imbalance. Recent advances highlight the potential of the Graph-of-Graphs (GoG) paradigm [15], which represents each input graph as a GoG node in a higher-level graph, with edges between GoG nodes defined via pairwise similarity between corresponding input graphs. This inter-graph representation enables

*Corresponding Author †Equal Contribution

richer supervision: by embedding minority-class or small graphs within a broader context of similar graphs, GoG-based methods enhance representation learning beyond what is possible using only intra-graph features.

However, existing GoG approaches [15, 13] encounter three major challenges that prevent them from fully harnessing the potential of GoG: **Challenge 1:** Existing GoG methods treat edge homophily (see in Definition 1) purely as a post hoc evaluation metric rather than incorporating it as an optimization objective during construction so that the resulting GoGs lack theoretical guarantees and capability to capture inter-graph supervision. **Challenge 2:** The construction of GoG edges relies heavily on pairwise graph similarity, which is typically computed using graph kernels (e.g., Weisfeiler-Lehman subtree [16] and shortest path [18]) that prioritize structural features over semantic ones. This struggles to precisely represent semantic relationships between graphs and incurs high computational cost (e.g., $\mathcal{O}(N^2|\bar{V}|^4)$, where N is the number of input graphs and $|\bar{V}|$ is the average number of nodes per graph). **Challenge 3:** Existing methods adopt a one-shot k NN strategy for GoG construction, assigning a fixed number of neighbors k to each GoG node. However, this fixed k makes the resulting GoG’s edge homophily highly sensitive to the choice of k^2 . Moreover, the one-shot construction introduces inductive biases and prevents the model from dynamically refining inter-graph relationships, underscoring the need for a more flexible and iterative GoG construction process.

To address these challenges, we propose **SamGoG**, a homophily-driven framework, designed to efficiently construct multiple GoGs by importance-sampling in the presence of class and graph size imbalance and trains on them sequentially. **For Challenge 1**, we formulate GoG construction as a constrained optimization problem where node degrees are adaptively assigned (Section 3.1). We prove that prioritizing neighbors with better similarity quality can increase expected edge homophily. **For Challenge 2**, we investigate a learnable pairwise similarity function that jointly encodes structural and semantic features. This not only eliminates the overhead of kernel-based methods but also improves edge homophily by guiding the sampler to favor same-class neighbors. **For Challenge 3**, we propose: a) an adaptive GoG node degree allocation strategy that adjusts neighborhood size for each GoG node to achieve higher homophily under class and graph size imbalance (Section 3.1); and b) a dynamic and parallel sampling method that generates multiple GoGs to capture a wider range of graph-level interactions during training. This replaces one-shot k NN construction, reduces inductive bias, and allows inter-graph supervision (Section 3.3) to evolve throughout training.

Our contributions can be summarized as follows. **First**, we propose SamGoG, the first framework to formulate GoG construction as a constrained homophily maximization problem, theoretically establishing the relationship between node degree allocation and homophily maximization. Our analysis demonstrates that degree distributions prioritizing nodes with better quality of similarity enhance homophily stability under Lemma 1, providing a theoretical foundation for topology-adaptive sampling aligned with the class and graph size imbalances. **Second**, we design three complementary mechanisms for GoG construction: 1) a learnable pairwise graph similarity function replacing graph kernels, which serves as the importance metric for sampling, 2) an adaptive GoG node degree allocation strategy replacing fixed node degree in the k NN method, and 3) a dynamic sampling method replacing one-shot k NN construction to generate multiple GoGs during training. Compared to baselines, ours improves edge homophily by over 5%, while achieving a 4-6 order of magnitude reduction in similarity computation time. **Third**, SamGoG achieves state-of-the-art (SOTA) performance on imbalanced graph classification benchmarks [21], demonstrating significant improvements across diverse datasets. Specifically, it outperforms baselines with an average accuracy increase of 5.07% in 24 class imbalance experiments across 4 datasets, and an average accuracy gain of 4.13% in 24 graph size imbalance experiments on the same datasets. Moreover, SamGoG achieves up to a $6.7\times$ acceleration over baselines. These results underscore SamGoG’s outstanding performance in both accuracy and efficiency.

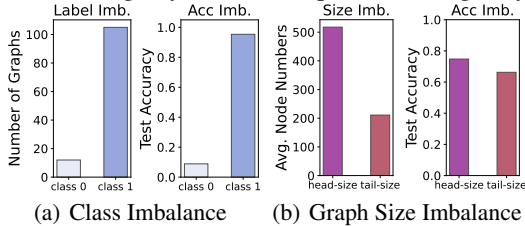


Figure 1: **Imbalanced training data results in biased model performance in D&D [16] (GIN [17]):** In (a), with only 10% of training graphs in class 0, the model shows significantly lower accuracy in that class. In (b), splitting test graphs by size shows that larger (head-size) graphs are generally easier to classify.

²When applying G²GNN [15] with the shortest path kernel to the PTC-MR [19] and DHFR [20] datasets (containing 344 and 756 graphs, respectively), increasing k from 1 to 10 leads to a notable drop in edge homophily—by 9% on PTC-MR and 15% on DHFR.

2 Preliminary

Graph-of-Graphs. The GoG represents a set of input graphs as nodes of a higher-order graph, therefore converting the problem of *graph classification* (assigning labels to input graphs) into a *semi-supervised node classification* task (assigning labels to GoG nodes).

Formally, given a set of N input graphs $\mathbb{G} = \{g_i\}_{i=1}^N$, let \mathbb{G}_L and $\mathbb{G}_U = \mathbb{G} \setminus \mathbb{G}_L$ denote the labeled and unlabeled subsets, respectively. Each input graph $g_i = (A_i, X_i, y_i) \in \mathbb{G}$ has s_i nodes (i.e., as graph size). The GoG is constructed as a high-order graph $G = (V, E, H, Y)$, where: (1) each GoG node $v_i \in V$ corresponds to an input graph $g_i \in \mathbb{G}$; (2) the GoG node feature $h_i \in H$ is encoded as $h_i = \text{Readout}(\mathcal{M}(A_i, X_i))$, where $\mathcal{M}(\cdot)$ denotes a GNN for node encoding and $\text{Readout}(\cdot)$ (e.g., mean/sum pooling [22, 17]) aggregates node embeddings; (3) GoG edges E capture relationships between input graphs (e.g., similarity); and (4) labels of GoG nodes $Y = \{y_i\}_{i=1}^N$ correspond directly to the labels of the original input graphs. Only the labels associated with the labeled subset $\{y_j \mid g_j \in \mathbb{G}_L\}$ are observable, while the labels $\{y_k \mid g_k \in \mathbb{G}_U\}$ remain unobserved and are the targets to be predicted.

The core of GoG construction lies in building the edge set E based on a precomputed pairwise graph similarity matrix $S \in \mathbb{R}^{N \times N}$. This process involves two key steps: 1) **Neighborhood Selection**: determine the count of edge connections k_i for each GoG node v_i , defining its neighborhood size. 2) **Edge Materialization**: for each v_i , update edge set E by adding directed edges from v_i to its k_i most similar counterparts in the GoG, as determined by the pairwise similarity matrix S .

Related Works. GoG extends the conventional GNN paradigm [23]. Early works like NoN [24] and GoGNN [25] introduce GoG for graph classification and link prediction, respectively. G²GNN [15] advances this idea by constructing a k NN-based GoG using graph similarity, alleviating class imbalance in graph classification via inter-graph message passing. Building on G²GNN, ImbGNN [13] introduces a similarity-aware graph random walk to extract core subgraphs, enhancing the reliability of kernel-based similarity under graph size imbalance. This enhancement addresses G²GNN’s limitation in underestimating similarity between graphs of different sizes but results in poorer efficiency due to the cost of extracting core subgraphs and more computation in pairwise similarity.

3 SamGoG

Framework. This section introduces the SamGoG, a sampling-based GoG framework for imbalanced graph classification by optimizing edge homophily, as shown in Figure 2. The detailed process is depicted in Algorithm 1. Initially, SamGoG calculates the GoG node degree (k_i) for all training graphs based on the three rules investigated in Section 3.2. Then, SamGoG embeds the input graphs with GNN encoders to obtain graph representations, i.e., GoG node embeddings (Line 3). Next, a multi-layer

Algorithm 1 SamGoG Pipeline

- 1: Pre-compute GoG node degree k_i for all training graphs via three rules
 - 2: **for** each training epoch **do**
 - 3: Obtain GoG node representations H
 - 4: Calculate pairwise similarity matrix S based on H via Equation (3)
 - 5: Perform parallel sampling and construct GoGs based on node degrees $\{k_i\}$ and the similarity matrix S
 - 6: Obtain label prediction based on downstream models
 - 7: Calculate loss function and back propagation
 - 8: **end for**
-

perceptron computes pairwise graph similarity matrix $S \in \mathbb{R}^{N \times N}$ between graph representations (Line 4). We then perform parallel sampling from an implicit complete graph³, guided by the node degrees $\{k_i\}$ and the similarity matrix S (Line 5). Each GoG node’s degree determines how many neighbors it selects in the sampled sub-GoG, while S defines the connection probabilities between node pairs. This process generates multiple sub-GoGs. Finally, these sampled sub-GoGs are used for training downstream backbone models (Line 6).

The rest of this section proceeds as follows. §3.1 formulates the GoG construction optimization objective based on edge homophily. §3.2 presents the methods of pairwise graph similarity computation and GoG node degree allocation. §3.3 analyzes subgraph training effectiveness on sampled GoGs and the complexity of several key components in the framework.

³The implicit complete graph, where edge weights are defined by pairwise similarity. [15, 13, 26].

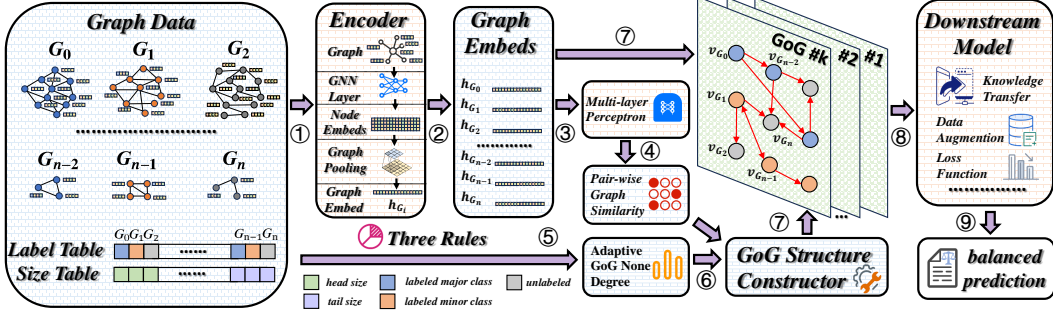


Figure 2: **Overview of SamGoG**: ① Input graphs to elemental GNN encoders; ② Output graph representations; ③ Use an MLP to compute the classification logits; ④ Compute pair-wise graph similarity matrix; ⑤ Adaptively allocate node degree for GoG nodes by class and size information; ⑥ Construct GoGs by importance sampling based on pair-wise graph similarity and adaptive node degree; ⑦ Combine GoG node features and sampled structure; ⑧ Train node classification model on constructed GoGs; ⑨ Output final result.

3.1 Graph-of-Graphs Construction Objective

We begin by defining the objective of GoG construction. Edge homophily is a widely acknowledged metric for evaluating the quality of GoG construction in existing works [15, 13]. Motivated by this, our goal is to maximize **edge homophily** [27] of constructed GoGs. It is worth noting that homophily can be defined in multiple ways [28, 27, 29]. To avoid ambiguity, we use “**homophily**” to specifically refer to edge homophily throughout this paper. Homophily is defined as follows:

Definition 1. (Homophily [27]): Given a GoG graph $G = (V, E, H, Y)$, the homophily of G ($\text{homo}(G)$) is defined as the fraction of edges linking two GoG nodes with the same label. Formally, we have homophily:

$$\text{homo}(G) = \frac{1}{|E|} \sum_{(v_i, v_j) \in E} \mathbb{I}(y_i = y_j) \quad (1)$$

, where $|E|$ denotes the number of edges. $\mathbb{I}(\cdot)$ denotes the indicator function that returns 1 when $y_i = y_j$, and 0 otherwise.

However, directly optimizing the homophily defined in Definition 1 is an optimization problem without constraints on node degrees, which harms GNN performance by incurring message-passing bottlenecks [30, 31]. In response, we design a constrained optimization that maximizes homophily subject to node degree constraints, as shown below.

$$\begin{aligned} \text{maximize} \quad \mathbb{E}(\text{homo}(G)) &= \frac{\sum_i k_i \cdot \text{prob}(v_i, y_i)}{\sum_i k_i} \\ \text{s.t.} \quad k_{\min} &\leq k_i \leq k_{\max} \quad \forall i \quad \text{and} \quad \sum_i k_i = N\bar{d} \end{aligned} \quad (2)$$

, where $\text{prob}(v_i, y_i) = \sum_{y_j \in Y} \mathbb{I}(y_j = y_i) \cdot \frac{S[i, j]}{\sum_k S[i, k]}$ denotes the homophily probability that GoG node v_i connects to neighbors with the same label y_i , based on the similarity matrix S . Here, \bar{d} is the target average GoG node degree, which is a pre-defined parameter. k_{\min} and k_{\max} are user-defined bounds that constrain the range of GoG node degrees. N is the number of input graphs, which is also the number of GoG nodes. $\sum_i k_i = N\bar{d}$ ensures that the sum of GoG node degrees is a fixed value, i.e., $N\bar{d}$.

Key Insights. Based on this optimization objective in Equation (2), two critical factors emerge as essential for improving the quality of sampling-based GoG construction. **First**, improving the quality of pairwise graph similarity, i.e., enhancing the similarity among GoG nodes sharing the same label, contributes to a higher value of $\text{prob}(v_i, y_i)$. **Second**, optimizing the distribution of GoG node degrees $\{k_i\}$ can further improve homophily: GoG nodes with higher $\text{prob}(v_i, y_i)$ should be assigned higher degrees k_i to maximize the overall homophily.

This leads us to a fundamental partial ordering principle, which provides a simplified yet effective solution to the optimization problem:

Lemma 1. For any two GoG nodes v_i and v_j with degrees k_i and k_j , if $\mathbb{E}(\text{prob}(v_i, y_i)) > \mathbb{E}(\text{prob}(v_j, y_j))$, then achieving optimal homophily in Equation (2) requires $k_i > k_j$. Conversely, if $\mathbb{E}(\text{prob}(v_i, y_i)) \leq \mathbb{E}(\text{prob}(v_j, y_j))$, then $k_i \leq k_j$ leads to better homophily.

Lemma 1 is proven in Section C.1. Lemma 1 establishes a relationship between homophily, degree allocation, and expected homophily probability. This principle allows us to prioritize higher degrees to GoG nodes with higher expected $\text{prob}(v_i, y_i)$, thereby improving the overall homophily in the GoG construction process.

3.2 Key Components

Pairwise Graphs-of-Graph Node Similarity Calculation

As shown in Algorithm 1, we first extract the feature representations of GoG nodes by employing a GNN (e.g., GIN [17] and GCN [4]). Through the message passing paradigm of GNNs, these feature representations capture the structural information present in the training graphs. Based on these representations, we further use an MLP-based method to encode the GoG nodes and get initial classification logits ($\text{logits}(g_i)$). To further take into account the label information of the training graphs, we calculate the similarity by incorporating labeled certainty and unlabeled uncertainty, as shown in Equation (3).

$$S[i, j] = P(\hat{y}_i) \cdot P(\hat{y}_j) = \sum_{c \in \mathcal{C}} P(\hat{y}_i = c) P(\hat{y}_j = c) \quad (3)$$

$$P(\hat{y}_i) = \begin{cases} \text{onehot}(y_i), & g_i \in \mathbb{G}_L \\ \text{Softmax}(\text{logits}(g_i)), & g_i \notin \mathbb{G}_L \end{cases}$$

where $\text{logits}(g_i) \in \mathbb{R}^{|\mathcal{C}|}$, $P(\hat{y}_i) \in \mathbb{R}^{|\mathcal{C}|}$, and $\sum_{c \in \mathcal{C}} P(\hat{y}_i = c) = 1$. Equation (3) adjusts the GoG node similarity by incorporating labeled certainty and unlabeled uncertainty. For labeled graphs ($\{g_i | g_i \in \mathbb{G}_L\}$), we preserve ground-truth certainty through one-hot encoding, while for unlabeled graphs ($\{g_i | g_i \notin \mathbb{G}_L\}$), we maintain probability distributions for the prediction label \hat{y}_i . For two graphs g_i and g_j , the joint probability of sharing class c is $P(\hat{y}_i = c, \hat{y}_j = c) = P(\hat{y}_i = c)P(\hat{y}_j = c)$ because of the independent and identically distributed (i.i.d.) assumption as shown in [32, 33, 34]. The full similarity matrix $S \in \mathbb{R}^{N \times N}$ can be computed efficiently as a parallel matrix operation ($S = PP^T$). Then, S can be further used to guide importance sampling for GoG construction as shown in Line 5 of Algorithm 1.

Graphs-of-Graph Node Degree Pre-allocation

Lemma 1 demonstrates that enhancing homophily via degree allocation leads to improved model accuracy. Inspired by this, we propose three rules to allocate GoG node degrees based on these distinct perspectives: the labeled and unlabeled parts: the majority and minority class in the labeled part; head-size and tail-size graphs of the unlabeled part. Based on the constraints in Equation (2), we first assign k_{\min} degrees to each GoG node. The remaining $\Delta = N(\bar{d} - k_{\min})$ degrees are then allocated according to the following rules.

Motivation 1: Labeled and Unlabeled GoG Nodes. First, we design the rule based on the differences between labeled and unlabeled GoG nodes. Since labeled nodes incorporate accurate class information during similarity computation, they tend to achieve better representation than their unlabeled counterparts. Motivated by this, we design the label priority rule as follows.

Rule 1 (Label Priority). Given a hyperparameter ratio ρ_1 ($\rho_1 > 1$), we divide Δ degrees to Δ_L and Δ_U between all the labeled and unlabeled nodes that $\frac{\Delta_L/N_L}{\Delta_U/N_U} = \rho_1$. N_L and N_U are labeled graph numbers and unlabeled graph numbers, respectively.

We can explain why Rule 1 works from the perspective Lemma 1. Because our focus is solely on the impact of labeling, we control for other variables by considering a pair of GoG nodes, v_i (labeled) and v_j (unlabeled), that share the same true label. Under this setup, we find that $\mathbb{E}(\text{prob}(v_i, y_i)) > \mathbb{E}(\text{prob}(v_j, y_j))$ (Please refer to Appendix C.2 for details). Therefore, according to Lemma 1, assigning a higher degree to the labeled GoG node (i.e., setting $k_i > k_j$) will lead to increased homophily.

Motivation 2: Major and Minor Classes in the Labeled GoG Nodes. Secondly, we design the rule based on the differences between major and minor classes in the labeled part. We assume that there is no shift in the class distribution between the labeled and unlabeled portions. As shown in Figure 1(a),

major classes achieve higher accuracy compared to minor classes, which shows that major classes have better representation. Motivated by this, we design the class imbalance rule as follows.

Rule 2 (Class Imbalance). *Given a hyperparameter ratio $\rho_2 > 1$, we divide Δ_L degrees to Δ_{major} and Δ_{minor} between all labeled nodes in majority and minority classes, such that $\frac{\Delta_{\text{major}}}{\Delta_{\text{minor}}} = \rho_2$.*

Similarly, we can also explain why Rule 2 is effective through the lens of Lemma 1. Consider two labeled GoG nodes, v_i with label y_i from the majority class and v_j with label y_j from the minority class. We can get $\mathbb{E}(\text{prob}(v_i, y_i)) > \mathbb{E}(\text{prob}(v_j, y_j))$ as detailed in Appendix C.2. According to Lemma 1, assigning a higher degree to the GoG node from the majority class (i.e., setting $k_i > k_j$) will improve overall homophily.

Motivation 3: Size Distributions in the Unlabeled GoG Nodes. Thirdly, we design the rule based on the differences in the size distributions of the unlabeled GoG nodes.

As shown in Figure 1(b), The imbalanced graph size leads to imbalanced classification performance. GNNs struggle to generalize across graph sizes not well represented in the training set, particularly when extrapolating from small to big graphs. In scenarios without a significant size distribution shift, head-size graphs typically achieve better performance. ImbGNN [13] highlights that for graphs with significant size differences but similar semantic information and the same true label, graph kernel functions tend to underestimate their similarity, hindering cross-size knowledge transfer in GoG-based methods. To address this, we introduce a window-based strategy, in which higher degrees are assigned to GoG nodes whose sizes better align with the training graph size distribution. The measure of alignment in size is quantified using a size window.

Rule 3 (Size Adaptation). *Let $w_{\text{train}} = \{s_k | g_k \in \mathbb{G}_L\}$ denote the size distribution of training graphs and $2r$ be the window width. For each unlabeled node v_i with size s_i , define its size window $w_i = [s_i - r, s_i + r]$. The allocated degrees Δ_U are distributed in proportion with $|w_{\text{train}} \cap w_i|$ as weight, where $|w_{\text{train}} \cap w_i|$ counts training graphs within v_i 's size window.*

This rule is based on Lemma 1. For two unlabeled GoG nodes v_i and v_j , if $|w_{\text{train}} \cap w_i| > |w_{\text{train}} \cap w_j|$, then $\mathbb{E}(\text{prob}(v_i, y_i)) > \mathbb{E}(\text{prob}(v_j, y_j))$ (Section C.2). According to Lemma 1, assigning a higher degree to v_i (i.e., $k_i > k_j$) improves homophily by prioritizing nodes whose sizes are better aligned with the training distribution.

Since the entire allocation process does not require the learned node representations, the GoG node degree allocation can be performed offline, as shown in Line 1 of Algorithm 1.

In summary, the procedure is as follows: (1) allocate degrees between labeled and unlabeled nodes (Rule 1); (2) adjust class-wise degrees in the labeled subset (Rule 2); and (3) apply Rule 3 to the unlabeled subset. Finally, the allocated degrees ($\{k_i\}$) are further used to guide importance sampling for GoG construction as shown in Line 5 of Algorithm 1.

3.3 Analysis

Sampling Analysis. To establish theoretical guarantees, we analyze the relationship between sample size t (number of GoG constructions) and downstream performance.

Theorem 1. Convergence of Sampling. *Every sampled subgraph-based gradient constitutes an unbiased estimator of the full-graph objective's gradient. Therefore, GCN parameters $\Theta^{(t)}$ converge in expectation to Θ_{full} , satisfying $\lim_{t \rightarrow \infty} \mathbb{E}[H^{(t)}] = H_{\text{full}}$, where H_{full} denotes node representations trained on the complete similarity-weighted graph.*

Theorem 1 is proven in Section C.3. Theorem 1 shows that the performance of GoG sampling-based method depends on the number of GoG constructions. When t is sufficiently large, our sampling-based method can closely approximate full-graph training, which leverages all available information. However, training on the complete graph, while allowing for greater information utilization, also results in low training efficiency. In contrast, we achieve better efficiency by optimizing importance-sampling with adaptive GoG node degree and training in parallel. Therefore, the sampling-based method is a better choice.

Theorem 2. Variance Analysis with t . *With diminishing learning rates, $\text{Var}(\Theta^{(t)})$ remains bounded with scaling behavior $\mathcal{O}(1/t)$. Consequently, $\text{Var}(H^{(t)}) = \mathcal{O}\left(\frac{1}{t}\right)$, causing final embeddings to concentrate around the full-graph solution as t increases.*

Theorem 2 is proven in Section C.3. We additionally analyze the sampling based on variance as shown in Theorem 2. This variance-reduction property demonstrates that increasing sample size t reduces inductive bias, consistent with the law of large numbers. Our sampling framework is also highly scalable in practice with GPU-optimized operations. It completes GoG construction for batches of over 1,000 graphs within milliseconds, which is several orders of magnitude faster than computing individual graph embeddings.

Complexity Analysis. In SamGoG, we adopt TailGNN [31] as the downstream model for its effectiveness in knowledge transfer from high-degree to low-degree nodes. The additional computational overhead primarily stems from three components in GoG construction: pairwise graph similarity calculation, adaptive GoG node degree allocation, and the sampling-based construction of the GoG structure. Here, N represents the number of graphs, and $|\mathcal{C}|$ denotes the number of classes. For similarity calculation, we compute similarity via matrix multiplication, with a time complexity of $\mathcal{O}(N^2|\mathcal{C}|)$, which is significantly lower than graph kernel methods. The GoG node degree allocation algorithm assigns the total number of edges based on predefined rules, resulting in a time complexity of $\mathcal{O}(N)$. For sampling-based construction of the GoG structure, its time complexity on a single GoG node is $\mathcal{O}(N)$, primarily due to normalization and cumulative distribution function calculations. Since neighborhoods of all N GoG nodes are sampled and aggregated in parallel, the overall time complexity for constructing the GoG remains $\mathcal{O}(N)$. In comparison, the overall time complexity of SamGoG is $\mathcal{O}(N^2|\mathcal{C}|)$, while that of existing GoG methods with kernel-based similarity [15, 13] is $\mathcal{O}(N^2|\mathcal{V}|^3)$ [15], and other baseline methods [35, 9, 8, 14] are $\mathcal{O}(\sum_{i=1}^N (|\mathcal{V}_i| + |\mathcal{E}_i|))$, where $|\mathcal{V}_i|$ and $|\mathcal{E}_i|$ represent the number of nodes and edges in each graph.

4 Experiments

In this section, we conduct extensive experiments to answer the following research questions: **(RQ1)** Can SamGoG effectively enhance the overall performance of imbalanced graph classification? **(RQ2)** Can SamGoG help improve the classification performance on minority class and tail-size graphs? **(RQ3)** Can SamGoG construct GoGs with ideal edge homophily? **(RQ4)** Is SamGoG efficient enough on large-scale graph data?

4.1 Experiment Setup

Benchmark Settings. We evaluate SamGoG on standard imbalanced classification benchmarks, IGL-Bench [21]. Following IGL-Bench, we adopt TUDatasets [36] and ogbg-molhiv [37] as datasets; details are provided in Appendix B.1. We use the predefined splits of each dataset with varying class/graph size imbalance ratios (defined in Equations (4) and (5) in Appendix A). Our implementation uses either GIN [17] or GCN [4] as base encoders and employs TailGNN [31] as the downstream model. Other implementation details are provided in Appendix B.2.

Baselines. We compare against all graph classification baselines in IGL-Bench [21], with additional comparisons of our GoG construction against kernel-based methods [18, 16, 38, 39] in G²GNN [15].

Table 1: Accuracy (% \pm stddev) on datasets with changing class imbalance levels over 10 runs, encoded by GIN / GCN. **Red** and **Blue** highlight the best and second-best results respectively.

Algorithm	PTC-MR	D&D	IMDB-B	REDDIT-B	Algorithm	PTC-MR	D&D	IMDB-B	REDDIT-B
Balance ($\rho_{\text{class}} = 5 : 5$)					Balance ($\rho_{\text{class}} = 5 : 5$)				
GIN (bb.) [17]	50.43 \pm 2.69	64.04 \pm 3.79	66.05 \pm 2.57	76.66 \pm 4.80	GCN (bb.) [4]	48.62 \pm 7.12	63.97 \pm 4.09	59.76 \pm 1.78	66.65 \pm 1.06
G ² GNN [15]	53.70 \pm 3.87	66.07 \pm 2.27	61.91 \pm 3.77	72.34 \pm 2.76	G ² GNN [15]	44.35 \pm 4.32	61.47 \pm 7.70	58.35 \pm 3.47	67.02 \pm 2.55
TopoImb [8]	50.91 \pm 2.18	66.57 \pm 3.81	66.28 \pm 1.85	73.99 \pm 1.18	TopoImb [8]	50.61 \pm 6.39	56.13 \pm 4.61	49.52 \pm 1.01	58.62 \pm 6.52
DataDec [35]	54.05 \pm 4.85	64.46 \pm 1.88	64.09 \pm 5.75	79.29 \pm 8.18	DataDec [35]	54.23 \pm 4.16	63.10 \pm 2.62	58.20 \pm 4.05	69.08 \pm 4.49
ImGKB [14]	53.48 \pm 3.50	65.45 \pm 2.88	50.16 \pm 0.34	50.24 \pm 0.29	ImGKB [14]	52.83 \pm 5.45	64.93 \pm 4.44	50.15 \pm 0.39	50.29 \pm 0.19
SamGoG	59.71 \pm 2.12	72.59 \pm 1.93	69.27 \pm 1.53	77.74 \pm 0.50	SamGoG	59.49 \pm 2.68	75.13 \pm 0.90	71.70 \pm 0.79	80.05 \pm 0.23
Low Imbalance ($\rho_{\text{class}} = 7 : 3$)					Low Imbalance ($\rho_{\text{class}} = 7 : 3$)				
GIN (bb.) [17]	47.83 \pm 2.95	51.05 \pm 5.07	62.31 \pm 3.99	61.10 \pm 4.86	GCN (bb.) [4]	43.84 \pm 7.03	58.32 \pm 1.51	49.06 \pm 2.17	61.85 \pm 3.89
G ² GNN [15]	51.88 \pm 6.23	56.29 \pm 7.30	63.87 \pm 4.64	69.58 \pm 3.59	G ² GNN [15]	47.86 \pm 9.03	65.65 \pm 5.41	53.11 \pm 3.97	66.02 \pm 2.08
TopoImb [8]	44.86 \pm 3.52	49.97 \pm 7.24	59.95 \pm 5.19	59.67 \pm 7.30	TopoImb [8]	45.90 \pm 6.41	44.63 \pm 4.82	49.75 \pm 4.81	54.35 \pm 3.13
DataDec [35]	55.72 \pm 2.88	63.51 \pm 1.62	67.92 \pm 3.37	78.39 \pm 5.01	DataDec [35]	55.86 \pm 2.49	64.66 \pm 2.04	57.06 \pm 5.97	66.45 \pm 5.38
ImGKB [14]	50.11 \pm 5.95	65.85 \pm 3.70	47.74 \pm 0.29	48.57 \pm 2.14	ImGKB [14]	49.49 \pm 5.12	67.44 \pm 3.50	47.65 \pm 0.23	48.58 \pm 2.15
SamGoG	57.25 \pm 2.85	73.31 \pm 1.99	67.96 \pm 0.57	78.67 \pm 1.44	SamGoG	56.98 \pm 3.65	74.81 \pm 0.99	68.35 \pm 1.59	80.03 \pm 1.03
High Imbalance ($\rho_{\text{class}} = 9 : 1$)					High Imbalance ($\rho_{\text{class}} = 9 : 1$)				
GIN (bb.) [17]	39.42 \pm 1.87	41.54 \pm 6.57	53.57 \pm 3.21	55.56 \pm 7.85	GCN (bb.) [4]	40.58 \pm 7.61	42.48 \pm 2.61	45.09 \pm 0.18	54.39 \pm 5.16
G ² GNN [15]	46.52 \pm 9.94	55.38 \pm 15.60	59.44 \pm 6.49	63.22 \pm 4.67	G ² GNN [15]	41.78 \pm 7.61	44.59 \pm 4.72	56.40 \pm 1.71	65.08 \pm 3.08
TopoImb [8]	39.42 \pm 1.24	39.12 \pm 1.62	47.75 \pm 3.73	51.58 \pm 4.69	TopoImb [8]	40.17 \pm 2.21	36.50 \pm 1.44	46.18 \pm 3.06	52.21 \pm 3.56
DataDec [35]	58.69 \pm 3.10	65.77 \pm 2.71	66.30 \pm 6.70	77.72 \pm 5.12	DataDec [35]	55.41 \pm 3.37	65.07 \pm 2.40	58.58 \pm 5.07	65.56 \pm 8.61
ImGKB [14]	44.24 \pm 5.65	59.99 \pm 7.57	47.08 \pm 3.72	51.25 \pm 5.10	ImGKB [14]	45.98 \pm 8.71	58.21 \pm 10.60	46.06 \pm 2.74	51.23 \pm 5.09
SamGoG	58.81 \pm 2.30	71.94 \pm 1.73	66.66 \pm 2.25	78.41 \pm 1.63	SamGoG	59.49 \pm 1.26	66.90 \pm 1.83	61.55 \pm 1.30	76.71 \pm 1.30

Table 2: Accuracy ($\% \pm \text{stddev}$) on datasets with changing size imbalance levels over 10 runs, encoded by GIN / GCN. **Red** and **Blue** highlight the best and second-best results respectively.

Algorithm	PTC-MR	D&D	IMDB-B	REDDIT-B
Low level ρ_{size}	1.60	1.56	1.64	2.79
GIN (bb.) [17]	52.17 \pm 4.36	65.01 \pm 0.69	66.38 \pm 4.27	67.41 \pm 2.32
SOLT-GNN [9]	47.54 \pm 4.33	63.78 \pm 1.06	64.20 \pm 5.46	49.57 \pm 6.78
TopoImb [8]	49.71 \pm 1.98	65.16 \pm 1.76	66.00 \pm 2.41	69.47 \pm 3.70
SamGoG	53.86\pm2.12	68.22\pm2.40	66.82\pm0.85	72.20\pm4.24
Mid level ρ_{size}	2.90	2.53	2.11	4.92
GIN (bb.) [17]	51.38 \pm 6.78	61.46 \pm 2.43	65.08 \pm 5.78	68.32 \pm 1.77
SOLT-GNN [9]	53.04 \pm 3.91	63.33 \pm 1.86	69.38 \pm 1.23	73.51 \pm 1.14
TopoImb [8]	51.59 \pm 4.30	65.99 \pm 1.25	68.10 \pm 0.87	71.54 \pm 0.75
SamGoG	57.17\pm1.06	71.91\pm1.22	69.53\pm1.01	79.12\pm0.90
High level ρ_{size}	4.93	8.91	4.45	10.97
GIN (bb.) [17]	48.41 \pm 7.07	60.68 \pm 6.89	62.60 \pm 3.82	67.41 \pm 2.23
SOLT-GNN [9]	51.74 \pm 5.25	64.97 \pm 3.24	65.03 \pm 4.12	60.24 \pm 2.11
TopoImb [8]	51.96 \pm 1.16	64.16 \pm 2.96	66.75 \pm 0.91	69.14 \pm 4.83
SamGoG	59.13\pm1.32	69.15\pm1.87	67.13\pm1.89	72.31\pm2.07

Algorithm	PTC-MR	D&D	IMDB-B	REDDIT-B
Low level ρ_{size}	1.60	1.56	1.64	2.79
GCN (bb.) [4]	51.59 \pm 7.07	64.82 \pm 0.75	69.15 \pm 1.44	53.44 \pm 1.78
SOLT-GNN [9]	51.45 \pm 3.13	65.69 \pm 2.36	68.23 \pm 2.48	37.58 \pm 3.04
TopoImb [8]	46.74 \pm 1.57	56.18 \pm 2.10	68.20 \pm 0.70	56.94 \pm 3.23
SamGoG	52.83\pm0.90	71.06\pm3.54	70.53\pm0.87	72.60\pm1.72
Mid level ρ_{size}	2.90	2.53	2.11	4.92
GCN (bb.) [4]	50.00 \pm 5.87	63.99 \pm 2.16	67.95 \pm 2.82	67.96 \pm 0.89
SOLT-GNN [9]	56.23 \pm 0.84	62.78 \pm 1.33	70.25 \pm 1.15	61.95 \pm 5.55
TopoImb [8]	54.13 \pm 4.62	64.73 \pm 7.09	68.75 \pm 0.76	69.12 \pm 0.52
SamGoG	57.03\pm1.46	72.80\pm2.53	70.54\pm0.40	79.08\pm1.36
High level ρ_{size}	4.93	8.91	4.45	10.97
GCN (bb.) [4]	49.93 \pm 5.90	60.98 \pm 6.71	64.88 \pm 2.02	66.38 \pm 0.46
SOLT-GNN [9]	54.78 \pm 6.03	63.21 \pm 3.40	69.80\pm2.07	67.05 \pm 2.54
TopoImb [8]	51.81 \pm 1.26	69.66 \pm 1.92	66.60 \pm 0.91	69.09 \pm 1.00
SamGoG	59.71\pm1.46	74.65\pm1.45	69.38 \pm 0.30	77.29\pm1.26

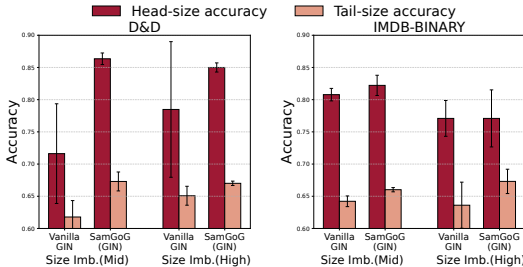


Figure 3: Test accuracy ($\pm \text{stddev}$) on head-/tail-size graphs by vanilla GIN and SamGoG with GIN as encoder.

4.2 Performance Analysis

To answer **RQ1**, as shown in Tables 1 and 2, SamGoG achieves state-of-the-art performance on 23/24 for both imbalance types, surpassing the second-best baseline by **5.07%** (class) and **4.13%** (size) in average accuracy. To answer **RQ2**, balanced accuracy and macro-F1 scores in Appendix E confirm consistent improvements across minority classes. For graph size imbalance, as shown in Figure 3, SamGoG simultaneously enhances accuracy on both head- and tail-size graphs compared to vanilla GIN [17], demonstrating effective mitigation of graph size imbalance. To confirm performance does not rely on the specific downstream model, we adopt GraphSHA [40] as an additional model on D&D dataset. Results in Appendix E.3 demonstrates SamGoG’s potential to leverage various downstream models. Figure 4 reports the relationship between sample size t and accuracy.

4.3 Efficiency Studies

To answer **RQ4**, we measure the time needed for two key steps in the GoG pipeline: calculating the pairwise graph similarity matrix and building the GoGs by sampling. We test this on the TUDataset (about 2,000 graphs) and the ogbg-molhiv dataset (over 41,000 graphs). As shown in Figure 5, SamGoG achieves remarkable efficiency in pairwise similarity computation, completing the task in milliseconds on TUDataset series (about 1,000~2,000 graphs). This represents a significant improvement over graph kernel methods, which require seconds to minutes for preprocessing at comparable scales. SOLT-GNN [9] requires 2,276 seconds for preprocessing and 500 epochs training on REDDIT-B, while SamGoG with an equally-sized model completes in 340 seconds, achieving a $6.7\times$ speedup. The efficiency advantage is further demonstrated in Figure 7 and Table 3 on the largest ogbg-molhiv dataset. SamGoG achieves SOTA accuracy and macro-F1 while maintaining the shortest preprocessing time. In SamGoG, the additional overhead of GoG construction and downstream model training per epoch accounts for only 7% of the total epoch time, highlighting its exceptional efficiency. These results collectively underscore SamGoG’s superior performance in handling large-scale imbalanced graph datasets.

4.4 Ablation Studies

In this section, we perform systematic ablation studies to investigate the individual contributions of key components in SamGoG. As evidenced in the class imbalance experiment (Table 1), SamGoG significantly outperforms G^2 GNN [15], a result we attribute to its superior edge homophily compared

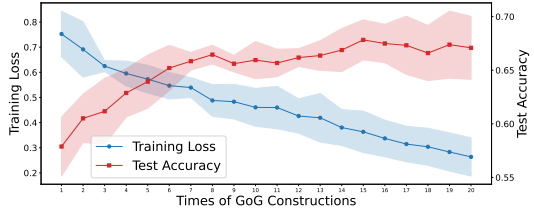


Figure 4: Train loss and test accuracy ($\pm \text{stddev}$) of SamGoG(GCN) on 20 times of GoG Constructions and downstream model training epochs on mid-level class imbalance split of D&D dataset.

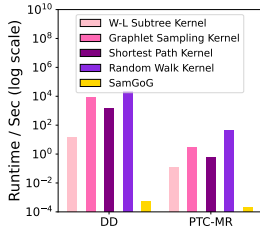


Figure 5: Runtime (seconds) of four kernel methods and SamGoG on D&D and PTC-MR GIN or GCN as encoder on 10%/25%/70% labeled data preserve competitive datasets.

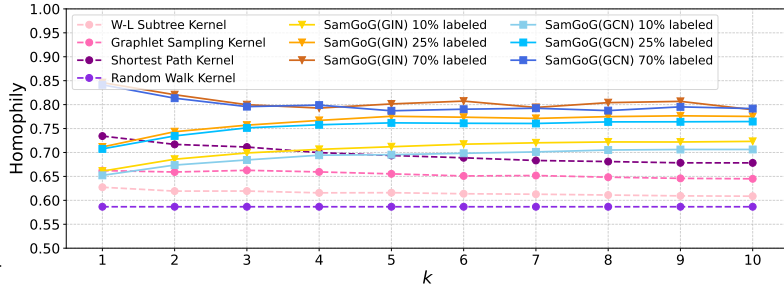


Figure 6: Edge homophily with different average degree k : SamGoG with on 10%/25%/70% labeled data preserve competitive edge and node homophily.

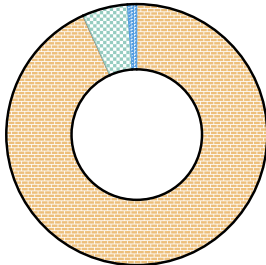


Figure 7: Runtime Proportion of SamGoG running on ogbg-molhiv dataset.

Table 3: Accuracy (% \pm stddev), Macro-F1 (% \pm stddev), average preprocessing time (second), and average epoch time (second) of graph classification on ogbg-molhiv dataset with low-level class-imbalanced split over 10 runs. “OOM” denotes out of memory or time limit.

Algorithm	Acc.	Macro-F1	Preprocessing Time (s)	Epoch Time (s)
Low Class Imbalance ($\rho_{\text{class}} = 20$)				
G ² GNN [15]	OOM	OOM	OOM	OOM
TopoImb [8]	OOM	OOM	OOM	OOM
DataDec [35]	OOM	OOM	OOM	OOM
SOLT-GNN [9]	OOM	OOM	OOM	OOM
ImGKB [14]	67.50 \pm 2.70	65.87 \pm 3.81	12.83	3.77
SamGoG	71.67\pm0.93	71.05\pm1.12	0.03	3.58

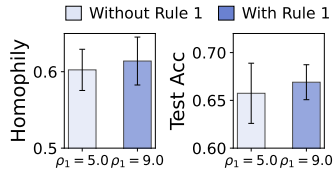


Figure 8: Edge Homophily (\pm std-dev) and test accuracy (\pm standard deviation) w/o and w/ Rule 1.

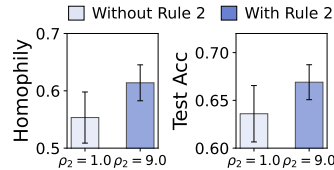


Figure 9: Edge Homophily (\pm std-dev) and test accuracy (\pm standard deviation) w/o and w/ Rule 2.

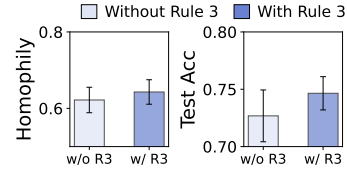


Figure 10: Edge Homophily (\pm stddev) and test accuracy (\pm standard deviation) w/o and w/ Rule 3.

to the kernel-based methods discussed in Figure 6. This also answer **RQ3**. To quantify the impact of our proposed node degree rules (Rules 1-3), we systematically evaluate three model variants by removing each rule independently. Specifically, we assess Rules 1 and 2 under the class-imbalanced partition of the D&D dataset, while Rule 3 is analyzed using the size-imbalanced partition. All experiments employ SamGoG with GCN as the backbone model, with mean and standard deviation metrics computed over 10 independent runs for both edge homophily and test accuracy. The ablation results (Figures 8, 9, and 10) demonstrate that the integration of all three rules yields a consistent improvement of several percentage points in both edge homophily synchronization and classification accuracy, thereby empirically validating their effectiveness.

5 Conclusion

This work introduces SamGoG, a sampling-based graph-of-graphs framework that effectively tackles class and graph size imbalance in graph classification. SamGoG enhances edge homophily of GoG by learnable pairwise graph similarity and adaptive GoG node degree allocation. The importance-based sampling mechanism ensures efficient construction of multiple GoGs and seamless integration with various downstream GNNs. SamGoG outperforms existing methods in both accuracy and efficiency.

References

- [1] Wenqi Fan, Yao Ma, Qing Li, Yuan He, Yihong Eric Zhao, Jiliang Tang, and Dawei Yin. Graph neural networks for social recommendation. In Ling Liu, Ryen W. White, Amin Mantrach, Fabrizio Silvestri, Julian J. McAuley, Ricardo Baeza-Yates, and Leila Zia, editors, *The World Wide Web Conference, WWW 2019*, pages 417–426. ACM.
- [2] Kanchan Jha, Sriparna Saha, and Hiteshi Singh. Prediction of protein–protein interaction using graph neural networks. *Scientific Reports*, 12(1):8360, 2022.
- [3] Hadi Abdine, Michail Chatzianastasis, Costas Bouyioukos, and Michalis Vazirgiannis. Prot2text: Multimodal protein’s function generation with gnns and transformers. pages 10757–10765.
- [4] Thomas N. Kipf and Max Welling. Semi-supervised classification with graph convolutional networks. In *5th International Conference on Learning Representations, ICLR 2017, Conference Track Proceedings*. OpenReview.net.
- [5] Petar Velickovic, Guillem Cucurull, Arantxa Casanova, Adriana Romero, Pietro Liò, and Yoshua Bengio. Graph attention networks. In *6th International Conference on Learning Representations, ICLR 2018, Conference Track Proceedings*. OpenReview.net.
- [6] Zhining Liu, Ruizhong Qiu, Zhichen Zeng, Hyunsik Yoo, David Zhou, Zhe Xu, Yada Zhu, Kommy Weldemariam, Jingrui He, and Hanghang Tong. Class-imbalanced graph learning without class rebalancing.
- [7] Shirui Pan and Xingquan Zhu. Graph classification with imbalanced class distributions and noise. In Francesca Rossi, editor, *IJCAI 2013, Proceedings of the 23rd International Joint Conference on Artificial Intelligence*, pages 1586–1592. IJCAI/AAAI.
- [8] Tianxiang Zhao, Dongsheng Luo, Xiang Zhang, and Suhang Wang. Topoimb: Toward topology-level imbalance in learning from graphs. In Bastian Rieck and Razvan Pascanu, editors, *Learning on Graphs Conference, LoG 2022*, volume 198 of *Proceedings of Machine Learning Research*, page 37. PMLR.
- [9] Zemin Liu, Qiheng Mao, Chenghao Liu, Yuan Fang, and Jianling Sun. On size-oriented long-tailed graph classification of graph neural networks. In Frédérique Laforest, Raphaël Troncy, Elena Simperl, Deepak Agarwal, Aristides Gionis, Ivan Herman, and Lionel Médini, editors, *WWW ’22: The ACM Web Conference 2022*, pages 1506–1516. ACM.
- [10] Nitesh V. Chawla, Kevin W. Bowyer, Lawrence O. Hall, and W. Philip Kegelmeyer. SMOTE: synthetic minority over-sampling technique. *J. Artif. Intell. Res.*, 16:321–357, 2002.
- [11] Chris Drummond, Robert C Holte, et al. C4. 5, class imbalance, and cost sensitivity: why under-sampling beats over-sampling. In *Workshop on learning from imbalanced datasets II*, volume 11, 2003.
- [12] Lirong Wu, Haitao Lin, Zhangyang Gao, Cheng Tan, and Stan Z. Li. Graphmixup: Improving class-imbalanced node classification on graphs by self-supervised context prediction, 2021.
- [13] Wei Xu, Pengkun Wang, Zhe Zhao, Binwu Wang, Xu Wang, and Yang Wang. When imbalance meets imbalance: Structure-driven learning for imbalanced graph classification. In Tat-Seng Chua, Chong-Wah Ngo, Ravi Kumar, Hady W. Lauw, and Roy Ka-Wei Lee, editors, *Proceedings of the ACM on Web Conference, WWW 2024*, pages 905–913. ACM.
- [14] Hui Tang and Xun Liang. Where to find fascinating inter-graph supervision: Imbalanced graph classification with kernel information bottleneck. In Abdulmotaleb El-Saddik, Tao Mei, Rita Cucchiara, Marco Bertini, Diana Patricia Tobon Vallejo, Pradeep K. Atrey, and M. Shamim Hossain, editors, *Proceedings of the 31st ACM International Conference on Multimedia, MM 2023*, pages 3240–3249. ACM.
- [15] Yu Wang, Yuying Zhao, Neil Shah, and Tyler Derr. Imbalanced graph classification via graph-of-graph neural networks. In Mohammad Al Hasan and Li Xiong, editors, *Proceedings of the 31st ACM International Conference on Information & Knowledge Management, 2022*, pages 2067–2076. ACM.

- [16] Nino Shervashidze, Pascal Schweitzer, Erik Jan van Leeuwen, Kurt Mehlhorn, and Karsten M. Borgwardt. Weisfeiler-lehman graph kernels. *J. Mach. Learn. Res.*, 12:2539–2561, 2011.
- [17] Keyulu Xu, Weihua Hu, Jure Leskovec, and Stefanie Jegelka. How powerful are graph neural networks? In *7th International Conference on Learning Representations, ICLR 2019, Conference Track Proceedings*. OpenReview.net.
- [18] Karsten M. Borgwardt and Hans-Peter Kriegel. Shortest-path kernels on graphs. In *Proceedings of the 5th IEEE International Conference on Data Mining (ICDM 2005)*, pages 74–81. IEEE Computer Society.
- [19] Yunsheng Bai, Hao Ding, Yang Qiao, Agustin Marinovic, Ken Gu, Ting Chen, Yizhou Sun, and Wei Wang. Unsupervised inductive graph-level representation learning via graph-graph proximity.
- [20] Jeffrey J. Sutherland, Lee A. O’Brien, and Donald F. Weaver. Spline-fitting with a genetic algorithm: A method for developing classification structure-activity relationships. *J. Chem. Inf. Comput. Sci.*, 43(6):1906–1915, 2003.
- [21] Jiawen Qin, Haonan Yuan, Qingyun Sun, Lyujin Xu, Jiaqi Yuan, Pengfeng Huang, Zhaonan Wang, Xingcheng Fu, Hao Peng, Jianxin Li, and Philip S. Yu. Igl-bench: Establishing the comprehensive benchmark for imbalanced graph learning.
- [22] David Duvenaud, Dougal Maclaurin, Jorge Aguilera-Iparraguirre, Rafael Gómez-Bombarelli, Timothy Hirzel, Alán Aspuru-Guzik, and Ryan P. Adams. Convolutional networks on graphs for learning molecular fingerprints. In Corinna Cortes, Neil D. Lawrence, Daniel D. Lee, Masashi Sugiyama, and Roman Garnett, editors, *Advances in Neural Information Processing Systems 28: Annual Conference on Neural Information Processing Systems 2015*, pages 2224–2232.
- [23] Jingchao Ni, Hanghang Tong, Wei Fan, and Xiang Zhang. Inside the atoms: ranking on a network of networks. In Sofus A. Macskassy, Claudia Perlich, Jure Leskovec, Wei Wang, and Rayid Ghani, editors, *The 20th ACM SIGKDD International Conference on Knowledge Discovery and Data Mining, KDD '14, 2014*, pages 1356–1365. ACM.
- [24] Shawn Gu, Meng Jiang, Pietro Hiram Guzzi, and Tijana Milenkovic. Modeling multi-scale data via a network of networks, 2022.
- [25] Hanchen Wang, Defu Lian, Ying Zhang, Lu Qin, and Xuemin Lin. Gognn: Graph of graphs neural network for predicting structured entity interactions. In Christian Bessiere, editor, *Proceedings of the Twenty-Ninth International Joint Conference on Artificial Intelligence, IJCAI 2020*, pages 1317–1323. ijcai.org.
- [26] Jiawen Qin, Pengfeng Huang, Qingyun Sun, Cheng Ji, Xingcheng Fu, and Jianxin Li. Graph size-imbalanced learning with energy-guided structural smoothing. In Wolfgang Nejdl, Sören Auer, Meeyoung Cha, Marie-Francine Moens, and Marc Najork, editors, *Proceedings of the Eighteenth ACM International Conference on Web Search and Data Mining, WSDM 2025*, pages 457–465. ACM.
- [27] Jiong Zhu, Yujun Yan, Lingxiao Zhao, Mark Heimann, Leman Akoglu, and Danai Koutra. Beyond homophily in graph neural networks: Current limitations and effective designs.
- [28] Hongbin Pei, Bingzhe Wei, Kevin Chen-Chuan Chang, Yu Lei, and Bo Yang. Geom-gcn: Geometric graph convolutional networks.
- [29] Derek Lim, Xiuyu Li, Felix Hohne, and Ser-Nam Lim. New benchmarks for learning on non-homophilous graphs, 2021.
- [30] Zemin Liu, Wentao Zhang, Yuan Fang, Xinming Zhang, and Steven C. H. Hoi. Towards locality-aware meta-learning of tail node embeddings on networks. In Mathieu d’Aquin, Stefan Dietze, Claudia Hauff, Edward Curry, and Philippe Cudré-Mauroux, editors, *CIKM '20: The 29th ACM International Conference on Information and Knowledge Management, 2020*, pages 975–984. ACM.

- [31] Zemin Liu, Trung-Kien Nguyen, and Yuan Fang. Tail-gnn: Tail-node graph neural networks. In Feida Zhu, Beng Chin Ooi, and Chunyan Miao, editors, *KDD '21: The 27th ACM SIGKDD Conference on Knowledge Discovery and Data Mining*, pages 1109–1119. ACM, 2021.
- [32] Charles Elkan. The foundations of cost-sensitive learning. In Bernhard Nebel, editor, *Proceedings of the Seventeenth International Joint Conference on Artificial Intelligence, IJCAI 2001*, pages 973–978. Morgan Kaufmann.
- [33] Abouzar Choubineh, David A. Wood, and Zahak Choubineh. Applying separately cost-sensitive learning and fisher’s discriminant analysis to address the class imbalance problem: A case study involving a virtual gas pipeline SCADA system. *Int. J. Crit. Infrastructure Prot.*, 29:100357, 2020.
- [34] Zhi-Hua Zhou and Xu-Ying Liu. Training cost-sensitive neural networks with methods addressing the class imbalance problem. *IEEE Trans. Knowl. Data Eng.*, 18(1):63–77, 2006.
- [35] Chunhui Zhang, Chao Huang, Yijun Tian, Qianlong Wen, Zhongyu Ouyang, Youhuan Li, Yanfang Ye, and Chuxu Zhang. When sparsity meets contrastive models: Less graph data can bring better class-balanced representations. In Andreas Krause, Emma Brunskill, Kyunghyun Cho, Barbara Engelhardt, Sivan Sabato, and Jonathan Scarlett, editors, *International Conference on Machine Learning, ICML 2023*, volume 202 of *Proceedings of Machine Learning Research*, pages 41133–41150. PMLR.
- [36] Christopher Morris, Nils M. Kriege, Franka Bause, Kristian Kersting, Petra Mutzel, and Marion Neumann. Tudataset: A collection of benchmark datasets for learning with graphs, 2020.
- [37] Weihua Hu, Matthias Fey, Marinka Zitnik, Yuxiao Dong, Hongyu Ren, Bowen Liu, Michele Catasta, and Jure Leskovec. Open graph benchmark: Datasets for machine learning on graphs.
- [38] Tamás Horváth, Thomas Gärtner, and Stefan Wrobel. Cyclic pattern kernels for predictive graph mining. In Won Kim, Ron Kohavi, Johannes Gehrke, and William DuMouchel, editors, *Proceedings of the Tenth ACM SIGKDD International Conference on Knowledge Discovery and Data Mining, 2004*, pages 158–167. ACM, 2004.
- [39] Natasa Przulj. Biological network comparison using graphlet degree distribution. *Bioinform.*, 23(2):177–183, 2007.
- [40] Wen-Zhi Li, Chang-Dong Wang, Hui Xiong, and Jian-Huang Lai. Graphsha: Synthesizing harder samples for class-imbalanced node classification. In Ambuj K. Singh, Yizhou Sun, Leman Akoglu, Dimitrios Gunopulos, Xifeng Yan, Ravi Kumar, Fatma Ozcan, and Jieping Ye, editors, *Proceedings of the 29th ACM SIGKDD Conference on Knowledge Discovery and Data Mining, KDD 2023*, pages 1328–1340. ACM.
- [41] Chen Cai and Yusu Wang. A simple yet effective baseline for non-attribute graph classification, 2018.
- [42] Pinar Yanardag and S. V. N. Vishwanathan. Deep graph kernels. In Longbing Cao, Chengqi Zhang, Thorsten Joachims, Geoffrey I. Webb, Dragos D. Margineantu, and Graham Williams, editors, *Proceedings of the 21th ACM SIGKDD International Conference on Knowledge Discovery and Data Mining, 2015*, pages 1365–1374. ACM.
- [43] Zhenqin Wu, Bharath Ramsundar, Evan N. Feinberg, Joseph Gomes, Caleb Geniesse, Aneesh S. Pappu, Karl Leswing, and Vijay S. Pande. Moleculenet: A benchmark for molecular machine learning. *CoRR*, abs/1703.00564, 2017.
- [44] Adam Paszke, Sam Gross, Francisco Massa, Adam Lerer, James Bradbury, Gregory Chanan, Trevor Killeen, Zeming Lin, Natalia Gimelshein, Luca Antiga, Alban Desmaison, Andreas Köpf, Edward Z. Yang, Zachary DeVito, Martin Raison, Alykhan Tejani, Sasank Chilamkurthy, Benoit Steiner, Lu Fang, Junjie Bai, and Soumith Chintala. Pytorch: An imperative style, high-performance deep learning library.
- [45] Matthias Fey and Jan Eric Lenssen. Fast graph representation learning with pytorch geometric. volume abs/1903.02428, 2019.

Contents of Appendix

A Imbalance Formulations	14
A.1 Class Distribution Imbalance	14
A.2 Graph Size Imbalance	14
B Details of the datasets and Experiments settings	14
B.1 Dataset Descriptions	14
B.2 Experimental Details	15
C Proofs of theorems	15
C.1 Analysis on Edge Homophily Optimization in Graph-of-Graphs Construction . . .	15
C.2 Three Rules In Sample Size	16
C.3 Effectiveness of Subgraph Training On Sequence of Sampled GoGs	19
D Limitations and Broader impacts	21
E Additional Results on IGL-Bench	22
E.1 Performance of Class Imbalance Classification	22
E.2 Performance of Graph Size Imbalance Classification	28
E.3 Performance on Different Downstream Models	31

A Imbalance Formulations

A.1 Class Distribution Imbalance

Given the labeled training set $\mathbb{G}_L = \{g_i\}_{i=1}^{N_L}$ where each graph g_i belongs to class $y_i \in \mathcal{C}$, we define the class imbalance ratio as:

$$\rho_{\text{class}} = \frac{\max_{c \in \mathcal{C}} |\{g_i \in \mathbb{G}_L | y_i = c\}|}{\min_{c \in \mathcal{C}} |\{g_i \in \mathbb{G}_L | y_i = c\}|} \quad (4)$$

This formulation captures the disparity between the most and least frequent classes in the training data. In practice, such imbalance leads to biased classifiers that favor majority classes, typically manifesting as low recall rates for minority classes where predictions disproportionately favor the dominant categories.

A.2 Graph Size Imbalance

For the complete graph dataset $\mathbb{G} = \{g_i\}_{i=1}^N$ where each graph g_i contains s_i nodes, we partition \mathbb{G} into head (\mathcal{H}_g) and tail (\mathcal{T}_g) sets containing the largest 20% and remaining 80% of graphs by size respectively. The size imbalance ratio is:

$$\rho_{\text{size}} = \frac{\frac{1}{|\mathcal{H}_g|} \sum_{g_i \in \mathcal{H}_g} s_i}{\frac{1}{|\mathcal{T}_g|} \sum_{g_j \in \mathcal{T}_g} s_j} \quad (5)$$

This structural imbalance creates two distinct challenges: (1) When training and test distributions are aligned, models underperform on tail-size graphs due to insufficient representation; (2) Under distribution shift, models exhibit degraded generalization when extrapolating to size regions sparsely represented in training.

B Details of the datasets and Experiments settings

B.1 Dataset Descriptions

We conducted the experiments on several datasets from the TUDataset series [36] and the ogbg-molhiv dataset from OGB Benchmark [37]. We use the same train/valid/test dataset splits created by IGL-Bench [21]. Detailed descriptions of datasets are as follows.

PTC-MR [19] is a dataset of 344 organic molecules represented as graphs, labeled for their mutagenic activity on bacteria and their carcinogenic effects on male rats. It is used for chemical compound classification and toxicity prediction, with an unspecified license.

D&D [16] contains over 1,000 protein structures represented as graphs, where nodes are amino acids and edges connect pairs within 6Å. The label indicates whether a protein is an enzyme. The dataset has an unspecified license.

IMDB-BINARY [41] is a movie collaboration dataset where nodes represent actors/actresses and edges indicate co-appearances in the same movie. The dataset is licensed under Creative Commons 4.0.

REDDIT-BINARY [42] is a balanced dataset where each graph represents an online discussion thread, with nodes as users and edges indicating reply interactions. The dataset is licensed under Creative Commons 4.0.

ogbg-molhiv [37] is a molecular graph classification dataset adopted from MoleculeNet [43] and is among the largest datasets in the collection. Each graph in the dataset represents a molecule, with nodes as atoms and edges as chemical bonds, and input node features are 9-dimensional, including atomic number, chirality, formal charge, and whether the atom is in a ring.

The information of the dataset can be viewed in Table 4. The input feature processing of the dataset follows the IGL Bench method. For the datasets PTC_MR and D&D, the unique hot code of node label is used. The dimension is the number of node label types, which are 18 and 89, respectively. For IMDB-BINARY and REDDIT-BINARY datasets without node labels, the unique hot code of node degree is used as the input feature, which is 135 and 3062 respectively. The ogbg-molhiv dataset is processed according to the standard method of the OGB Benchmark.

Table 4: Statistics of benchmark datasets for graph classification.

Dataset	#Graphs	Avg. #Nodes	Avg. #Edges	#Classes	#Node Labels	#Edge Labels	#Node Attrs	#Edge Attrs
PTC-MR	344	14.3	14.7	2	+	+	-	-
D&D	1,178	284.3	715.7	2	+	-	-	-
IMDB-BINARY	1,000	19.8	96.5	2	-	-	-	-
REDDIT-BINARY	2,000	429.6	497.8	2	-	-	-	-
ogbg-molhiv	41,127	25.5	27.5	2	-	-	+(9)	+(3)

B.2 Experimental Details

Computational Environment. All experiments were conducted using PyTorch [44] 2.4.0 with CUDA 12.4 and PyTorch-Geometric 2.6.1 [45].

Hyperparameter Ranges. Hyperparameters encompass three parts: (1) general settings, (2) GoG construction hyperparameters, and (3) downstream model hyperparameters. Hyperparameter Ranges are in Table 5.

Table 5: Hyperparameter search space for the experiments.

Parts	Hyperparameter	Search Space
General Settings	dropout	0.1, 0.2, 0.5
	weight decay	$0, 5 \times 10^{-6}, 5 \times 10^{-5}, 5 \times 10^{-4}, 5 \times 10^{-3}$
	number of max training epochs	500
	learning rate	0.001, 0.005, 0.01, 0.0125, 0.05
	number of layers	2, 3, 4
	hidden size	32, 64, 128
	batch size	128
GoG Construction	target average node degree \bar{d}	5, 8, 10
	minimum node degree k_{min}	0, 3, 5
	maximum node degree k_{min}	100
	ρ_1 in Rule 1	5, 9
	ρ_2 in Rule 2	1, 3, 9
r in Rule 3	2, 20, 50	
Downstream Tail-GNN [31]	number of dropped edges	3, 5
	μ for \mathcal{L}_m	0.01, 0.001
	η for \mathcal{L}_d	0.1, 1.0
Downstream GraphSHA [40]	sampled β -distribution	$\beta(1,100), \beta(1,10)$
	weighted algorithm	Personalized PageRank, Heat Kernel

Edge Homophily Analysis Protocol. We measure edge homophily ratio $\text{homo}(G) = \frac{\sum_{(i,j) \in E} \mathbb{1}(y_i=y_j)}{|E|}$ for GoG structures, comparing against baseline methods under identical initialization conditions. Evaluation metrics are computed over 10 random seeds to ensure statistical significance.

C Proofs of theorems

In this section, we provide the proof of the optimization objective modeling of edge homophily; the rationality of the three rules in GoG node degree allocation; and the quality analysis of sampled GoGs for downstream model training.

C.1 Analysis on Edge Homophily Optimization in Graph-of-Graphs Construction

Proof. Proof of Lemma 1.

Consider a GoG graph G with N nodes $V = \{v_1, v_2, \dots, v_N\}$, true labels $Y = \{y_1, \dots, y_N\}$, and $\text{prob}(v_i, y_i) = \sum_{y_j \in Y} \mathbb{1}(y_j = y_i) \cdot \frac{S[i,j]}{\sum_k S[i,k]}$. The graph-of-graphs is constructed such that the average out-degree is constant K . The sample size distribution $k = \{k_1, \dots, k_N\}$ satisfies

$\sum_i k_i = N\bar{d}$, and the goal is to maximize the expected edge homophily as expressed in Equation (2):

$$\mathbb{E}(\text{homo}(G)) = \frac{\sum_i k_i \cdot \text{prob}(v_i, y_i)}{N\bar{d}}. \quad (6)$$

Since the denominator in Equation (6) is constant, the problem reduces to maximizing the numerator $\sum_i k_i \cdot \text{prob}(v_i, y_i)$. This can be viewed as a weight allocation problem. Let $t(1), t(2), \dots, t(n)$ denote an arrangement of indices such that:

$$\text{prob}(v_{t(1)}, y_{t(1)}) \leq \text{prob}(v_{t(2)}, y_{t(2)}) \leq \dots \leq \text{prob}(v_{t(N)}, y_{t(N)}). \quad (7)$$

The problem is equivalent to assigning weights $\omega_i = \frac{k_i}{N\bar{d}}$ such that $\sum_i \omega_i = 1$. It is evident that the optimal solution, under no constraints, is:

$$\begin{aligned} \omega_{t(1)} = \omega_{t(2)} = \dots = \omega_{t(N-1)} = 0, \quad \omega_{t(N)} = 1, \\ k_{t(1)} = k_{t(2)} = \dots = k_{t(n-1)} = 0, \quad k_{t(n)} = N\bar{d}. \end{aligned} \quad (8)$$

However, practical constraints such as non-zero sample sizes and a degree distribution suitable for GNN training impose limits on skewness. Let $k^{opt} = \{k_i^{opt} : 1 \leq i \leq N\}$ denote a sample size sequence satisfying $\sum_i k_i^{opt} = N\bar{d}$ and $k_1^{opt} \leq k_2^{opt} \leq \dots \leq k_N^{opt}$. By the rearrangement inequality, for any permutation σ of $\{1, 2, \dots, n\}$ and any $\{k_i\}$ satisfying $\sum_1^N k_i = N\bar{d}$:

$$\begin{aligned} k_1^{opt} \cdot \text{prob}(v_{t(1)}) + k_2^{opt} \cdot \text{prob}(v_{t(2)}) + \dots + k_N^{opt} \cdot \text{prob}(v_{t(N)}) \\ \geq k_{\sigma(1)} \cdot \text{prob}(v_{t(1)}) + k_{\sigma(2)} \cdot \text{prob}(v_{t(2)}) + \dots + k_{\sigma(N)} \cdot \text{prob}(v_{t(N)}). \end{aligned} \quad (9)$$

For any two nodes v_i and v_j such that $\mathbb{E}[\text{prob}(v_i, y_i)] > \mathbb{E}[\text{prob}(v_j, y_j)]$ but $k_i < k_j$, exchanging their sample sizes increases edge homophily. Thus, the sample size distribution that maximizes homophily aligns with the $\text{prob}(\cdot)$ ranking of nodes. \square

C.2 Three Rules In Sample Size

Proof. Proof of Rule 1[**Label Priority**].

Consider two graph nodes v_i and v_j in the graph-of-graphs (GoGs), with ground truth labels $y_i = y_j = 0$. Node v_i is labeled, while v_j is unlabeled. Their predicted probabilities are:

$$P(\hat{y}_i) = (1, 0), \quad P(\hat{y}_j) = (x, 1-x), \quad x \in (0, 1). \quad (10)$$

From Equation (3), and $\text{prob}(v_i, y_i) = \sum_{G_j \in \mathcal{G}} \mathbb{I}(y_j = y_i) \cdot \frac{S^{[i,j]}}{\sum_k S^{[i,k]}}$, the $\text{prob}(\cdot)$ value for node v_i is:

$$\begin{aligned} \mathbb{E}(\text{prob}(v_i, 0)) &= \frac{\mathbb{I}(y_k = 0) \sum_k S_{i,k}}{\sum_k S_{i,k}} \\ &= \frac{(\sum_{j, y_j=0} P(\hat{y}_k = 0))P(\hat{y}_i = 0) + (\sum_{k, y_k=0} P(\hat{y}_k = 1))P(\hat{y}_i = 1)}{(\sum_{k, y_k=0} P(\hat{y}_k = 0) + \sum_{k, y_k=1} P(\hat{y}_k = 0))P(\hat{y}_i = 0) + (\sum_{k, y_k=0} P(\hat{y}_k = 1) + \sum_{k, y_k=1} P(\hat{y}_k = 1))P(\hat{y}_i = 1)} \end{aligned} \quad (11)$$

For ease of expression, we denote four constants:

$$\begin{aligned} \gamma_0^0 &= \sum_{j, y_k=0} P(\hat{y}_k = 0), \gamma_0^1 = \sum_{k, y_k=0} P(\hat{y}_k = 1), \\ \gamma_1^0 &= \sum_{j, y_k=1} P(\hat{y}_k = 0), \gamma_1^1 = \sum_{k, y_k=1} P(\hat{y}_k = 1) \end{aligned} \quad (12)$$

the subscript indicates the true label, and the superscript indicates the predicted label. Therefore, we have,

$$\begin{aligned} \gamma_0^0 + \gamma_0^1 &= \sum_{k, y_k=0} 1 \\ \gamma_1^0 + \gamma_1^1 &= \sum_{k, y_k=1} 1 \end{aligned} \quad (13)$$

For a well trained MLP for binary classification, we assume that the prediction probability of all samples of each class belonging to its own true label is higher than that of the other class, so they satisfy:

$$\begin{aligned} 0 < \gamma_0^1 < \gamma_0^0 \\ 0 < \gamma_1^0 < \gamma_1^1. \end{aligned} \quad (14)$$

Let's rewrite the Equation (11) as a function of $P(\hat{y}_i = 0)$,

$$\begin{aligned} \mathbb{E}(\text{prob}(v_i, 0)) = f_0(P(\hat{y}_i = 0)) &= \frac{\gamma_0^0 P(\hat{y}_i = 0) + \gamma_0^1 (1 - P(\hat{y}_i = 0))}{(\gamma_0^0 + \gamma_1^0) P(\hat{y}_i = 0) + (\gamma_0^1 + \gamma_1^1) (1 - P(\hat{y}_i = 0))}, \\ f_0(x) &= \frac{\gamma_0^0 x + \gamma_0^1 (1 - x)}{(\gamma_0^0 + \gamma_1^0) x + (\gamma_0^1 + \gamma_1^1) (1 - x)} \end{aligned} \quad (15)$$

Differentiating $f_0(x)$:

$$f_0'(x) = \frac{\gamma_0^0 \gamma_1^1 - \gamma_0^1 \gamma_1^0}{[(\gamma_0^0 + \gamma_1^0) x + (\gamma_0^1 + \gamma_1^1) (1 - x)]^2} \quad (16)$$

According to Equation (14), we have,

$$\gamma_0^0 \gamma_1^1 - \gamma_0^1 \gamma_1^0 > 0 \Rightarrow f_0'(x) > 0 \quad (17)$$

Since $f_0'(x) > 0$, making $f_0(x)$ an increasing function. Thus, for labeled v_i and unlabeled v_j :

$$\begin{aligned} P(\hat{y}_i = 0) = 1 > P(\hat{y}_j = 0) &\implies f_0(P(\hat{y}_i = 0)) > f_0(P(\hat{y}_j = 0)) \\ &\implies \mathbb{E}[\text{prob}(v_i, 0)] > \mathbb{E}[\text{prob}(v_j, 0)]. \end{aligned} \quad (18)$$

By symmetry, the conclusion holds for class 1. From Lemma 1, a higher score implies $k_i > k_j$ for better homophily. \square

Proof. Proof of Rule 2[**Class Imbalance**].

We analyze and compare the expected scores $\mathbb{E}[\text{prob}(v_i, y_i = 0)]$ and $\mathbb{E}[\text{prob}(v_j, y_j = 1)]$ in the context of binary classification ($y \in \{0, 1\}$) under three imbalanced training/testing scenarios. The derivation proceeds in six steps.

Step 1: Notation and Setup.

Let \mathbb{G}_L be the labeled training set, and \mathbb{G}_U the unlabeled part. Denote the class sizes:

$$\begin{aligned} T_0^L &= |\{g_i \in \mathbb{G}_L : y_i = 0\}|, & T_1^L &= |\{g_i \in \mathbb{G}_L : y_i = 1\}|, \\ T_0^U &= |\{g_j \in \mathbb{G}_U : y_j = 0\}|, & T_1^U &= |\{g_j \in \mathbb{G}_U : y_j = 1\}|, \\ N_0^U + N_1^U &= N^U = |\mathbb{G}_U|, & N_0^L + N_1^L &= N^L = |\mathbb{G}_L|. \end{aligned} \quad (19)$$

For each test sample $g_a \in \mathbb{G}_U$, $P(\hat{y}_a) = (P(\hat{y}_a = 0), P(\hat{y}_a = 1))$ denote the predicted probabilities for classes 0 and 1 such that $P(\hat{y}_a = 0) + P(\hat{y}_a = 1) = 1$.

Step 2: Precise Definition of $\mathbb{E}[\text{prob}(v_a, y_a)]$.

The similarity matrix S is defined as $S = PP^T$, with elements:

$$\begin{aligned} S[a, b] &= P(\hat{y}_a) \cdot P(\hat{y}_b) = \sum_{c \in \{0, 1\}} P(\hat{y}_a = c) P(\hat{y}_b = c) \\ P(\hat{y}_a) &= \begin{cases} \text{onehot}(y_a), & g_a \in \mathbb{G}_L \\ \text{Softmax}(\text{logits}(g_a)), & g_a \notin \mathbb{G}_L \end{cases} \end{aligned} \quad (20)$$

Step 3: Random Variables and Expectation.

For a training sample g_i and its corresponding GoG node v_i with $y_i = 0$, the score expands to:

$$\mathbb{E}[\text{prob}(v_i, y_i = 0)] = \frac{T_0^L + X_0^{\text{true}}}{T_0^L + \Omega_0}, \quad (21)$$

where:

$$X_0^{\text{true}} = \sum_{\substack{g_k \in \mathbb{G}_U \\ y_k = 0}} P(\hat{y}_k = 0), \quad \Omega_0 = \sum_{g_k \in \mathbb{G}_U} P(\hat{y}_k = 0). \quad (22)$$

Similarly, for g_j and its corresponding GoG node v_j with $y_j = 1$,

$$\mathbb{E}[\text{prob}(v_j, y_j = 1)] = \frac{T_1^L + X_1^{\text{true}}}{T_1^L + \Omega_1}, \quad (23)$$

where:

$$X_1^{\text{true}} = \sum_{\substack{g_k \in \mathbb{G}_U \\ y_k = 1}} P(\hat{y}_k = 1), \quad \Omega_1 = \sum_{g_k \in \mathbb{G}_U} P(\hat{y}_k = 1). \quad (24)$$

Step 4: Asymptotic Convergence and Concentration.

Assume the test samples $g_k \in \mathbb{G}_U$ are i.i.d. with class priors $\pi_0 = P(y_k = 0)$ and $\pi_1 = P(y_k = 1)$, such that $\pi_0 + \pi_1 = 1$. Let $\alpha_0 = \mathbb{E}[P(\hat{y}_k = 0) \mid y_k = 0]$ and $\alpha_1 = \mathbb{E}[P(\hat{y}_k = 1) \mid y_k = 1]$ denote the expected probabilities assigned to the correct classes. Applying the Law of Large Numbers (LLN):

$$X_0^{\text{true}} \approx \pi_0 \alpha_0 T^U, \quad \Omega_0 \approx (\pi_0 \alpha_0 + \pi_1 (1 - \alpha_1)) T^U.$$

Substituting these into $\mathbb{E}[\text{prob}(v_i, y_i = 0)]$ yields:

$$\mathbb{E}[\text{prob}(v_i, y_i = 0)] \approx \frac{T_0^L + \pi_0 \alpha_0 T^U}{T_0^L + (\pi_0 \alpha_0 + \pi_1 (1 - \alpha_1)) T^U}.$$

Step 5: Comparisons Across Scenarios.

We evaluate $\mathbb{E}[\text{prob}(v_i, y_i = 0)]$ and $\mathbb{E}[\text{prob}(v_j, y_j = 1)]$ under three scenarios:

- **Scenario 1: Class 0 is dominant in both training and testing.** Typically, $\alpha_0 > \alpha_1$ and $\pi_0 > \pi_1$, leading to:

$$\mathbb{E}[\text{prob}(v_i, y_i = 0)] > \mathbb{E}[\text{prob}(v_j, y_j = 1)].$$

- **Scenario 2: Balanced training, but class 0 dominates in testing.** Here, $\alpha_0 \approx \alpha_1$ and $\pi_0 > \pi_1$, implying:

$$\mathbb{E}[\text{prob}(v_i, y_i = 0)] \geq \mathbb{E}[\text{prob}(v_j, y_j = 1)].$$

- **Scenario 3: Class 0 is dominant in training, but class 1 dominates in testing.** The reversed class distribution and possible misclassification of truly 1 samples into 0 may result in:

$$\mathbb{E}[\text{prob}(v_i, y_i = 0)] < \mathbb{E}[\text{prob}(v_j, y_j = 1)].$$

Step 6: Conclusion. These results demonstrate the effect of training/testing imbalance on expected scores. The analysis can be extended to multi-class settings with more intricate assumptions and bounds. \square

Proof. Proof of Rule 3 (**Size Adaptation**).

Let $w_{\text{train}} = \{s_k \mid g_k \in \mathbb{G}_L\}$ denote the size distribution of training graphs and $2r$ be the window width. For each unlabeled node v_i with size s_i , define its size window $w_i = [s_i - r, s_i + r]$.

The *size-generalisation phenomenon* described in the main text is captured by the following assumption.

Assumption 1. For two unlabeled graphs g_i, g_j that share the same ground-truth label $y_i = y_j = c$, g_i has more probability to be classified than g_j due to $|w_{\text{train}} \cap w_i| > |w_{\text{train}} \cap w_j|$ according to GNN's size-generalisation phenomenon, therefore $P(\hat{y}_i = c) > P(\hat{y}_j = c)$.

Following the Equation (18) and Assumption 1, we have

$$\begin{aligned} P(\hat{y}_i = c) > P(\hat{y}_j = c) &\implies f_0(P(\hat{y}_i = c)) > f_0(P(\hat{y}_j = c)) \\ &\implies \mathbb{E}[\text{prob}(v_i, c)] > \mathbb{E}[\text{prob}(v_j, c)]. \end{aligned} \quad (25)$$

\square

C.3 Effectiveness of Subgraph Training On Sequence of Sampled GoGs

Proof. Effectiveness of GoG Training.

I. Problem Setting and Goals

Given a directed weighted graph $G = (V, E)$ with N nodes and a pairwise graph similarity matrix

$$S \in [0, 1]^{N \times N}, \quad (26)$$

as weights in importance-sampling, we have:

1. If two labeled nodes i and j belong to the same class, then $S[i, j] = 1$.
2. If two labeled nodes i and j belong to different classes, then $S[i, j] = 0$ (treated as no edge).
3. Otherwise, each edge weight $S[i, j]$ lies in the interval $[0, 1]$.

We employ a Graph Neural Network (GNN), for instance a GCN, for a semi-supervised node classification task on G . Since G can be almost a complete directed graph (potentially $O(N^2)$ edges), training a GCN directly on the full graph may be computationally expensive or memory intensive. Hence, we introduce a *sampling mechanism*:

- For each node i , we sample k_i outgoing edges.
- The probability of sampling edge (i, j) is proportional to its weight (similarity) $S[i, j]$.
- In the resulting sampled subgraph, each chosen edge is assigned weight 1, while edges not chosen are considered absent.

After sampling a subgraph in each round, we perform one forward pass and one backward pass (updating the GCN parameters). Repeating this for t rounds yields the final node embeddings $H^{(t)}$. Our goal is to prove:

- **Expectation Approximation:** The expected final embeddings $H^{(t)}$ approach those obtained by training a weighted GCN on the entire graph G , denoted H_{full} .
- **Variance Reduction:** As t grows, the variance of these embeddings decreases, typically at a rate on the order of $1/t$.

II. Sampling Mechanism and Subgraph Representation

(a) *Sampling Probabilities.*

In one sampling round, the probability of selecting edge (i, j) is

$$p_{i,j} = \frac{k_i S[i, j]}{\sum_m S[i, m]}. \quad (27)$$

We assume k_i is chosen so that such sampling is feasible.

(b) *Adjacency Matrix of the Sampled Subgraph.*

Define the adjacency matrix of the sampled subgraph in the s -th round by

$$A_s \in \{0, 1\}^{n \times n}, \quad (28)$$

where

$$A_s(i, j) = \begin{cases} 1, & \text{if edge } (i, j) \text{ is sampled,} \\ 0, & \text{otherwise.} \end{cases} \quad (29)$$

Then

$$\mathbb{E}[A_s(i, j)] = p_{i,j} = \frac{k_i S[i, j]}{\sum_m S[i, m]}. \quad (30)$$

(c) *Normalization.*

GCNs often use a normalized adjacency (e.g. $\hat{A} = D^{-\frac{1}{2}} A D^{-\frac{1}{2}}$). For the sampled subgraph, let

$$\hat{A}_s = \text{Norm}(A_s). \quad (31)$$

Under unbiased sampling assumptions, we typically have

$$\mathbb{E}[\hat{A}_s] \approx \hat{W} = \text{Norm}(W). \quad (32)$$

III. GCN Training via Randomized Subgraphs (SGD Perspective)

(a) *Parameterization and Loss Function.*

Let all GCN parameters be

$$\Theta. \quad (33)$$

We aim to minimize a loss function $\mathcal{L}(\Theta)$ over the full graph, for instance a cross-entropy for semi-supervised learning. The full gradient is

$$\nabla_{\Theta} \mathcal{L}_{\text{full}}(\Theta). \quad (34)$$

(b) *Unbiased Gradient Estimates.*

When we sample a subgraph A_s and compute a local loss $\mathcal{L}_s(\Theta)$, the resulting gradient

$$g_s = \nabla_{\Theta} \mathcal{L}_s(\Theta) \quad (35)$$

is designed to be an unbiased estimator of the full gradient:

$$\mathbb{E}[g_s] = \nabla_{\Theta} \mathcal{L}_{\text{full}}(\Theta). \quad (36)$$

(c) *Parameter Updates.*

In the s -th iteration, given learning rate η_s ,

$$\Theta^{(s)} = \Theta^{(s-1)} - \eta_s \nabla_{\Theta} \mathcal{L}_s(\Theta^{(s-1)}). \quad (37)$$

This matches the standard Stochastic Gradient Descent (SGD) framework.

IV. Expected Node Embeddings

(a) *Relationship Between Embeddings and Parameters.*

Let

$$f(\cdot; \Theta) : \mathbb{R}^{N \times d_0} \rightarrow \mathbb{R}^{N \times d_L} \quad (38)$$

denote the GCN forward mapping from input features X to embeddings. Then

$$H(\Theta) = f(X; \Theta). \quad (39)$$

Suppose Θ_{full} is the optimal parameter (in the full-graph sense), and

$$H_{\text{full}} = f(X; \Theta_{\text{full}}). \quad (40)$$

(b) *Convergence in Expectation.*

Under the unbiased gradient assumption and appropriate SGD theory (e.g. Robbins-Monro),

$$\Theta^{(s)} \rightarrow \Theta_{\text{full}} \quad \text{in expectation, as } s \rightarrow \infty. \quad (41)$$

Hence defining

$$H^{(t)} = f(X; \Theta^{(t)}), \quad (42)$$

we obtain

$$\lim_{t \rightarrow \infty} \mathbb{E}[H^{(t)}] = H_{\text{full}}, \quad (43)$$

assuming continuity of f . This proves $\mathbb{E}[H^{(t)}]$ converges to the full-graph solution.

V. Variance Analysis and Rate of Convergence

(a) *Parameter Variance.*

If

$$g_s = \nabla_{\Theta} \mathcal{L}_s(\Theta^{(s-1)}) \quad (44)$$

has variance bounded by Σ_0 , then the updates

$$\Theta^{(s)} = \Theta^{(s-1)} - \eta_s g_s \quad (45)$$

can be controlled by choosing a diminishing learning rate, for example $\eta_s = \eta_0/s$. Classical results show that

$$\text{Var}(\Theta^{(t)}) = \mathcal{O}\left(\frac{1}{t}\right). \quad (46)$$

(b) *Embedding Variance.*

For the node embeddings $H^{(t)} = f(X; \Theta^{(t)})$, if we linearize around Θ_{full} :

$$H^{(t)} \approx H_{\text{full}} + J_{\Theta_{\text{full}}} (\Theta^{(t)} - \Theta_{\text{full}}), \quad (47)$$

where $J_{\Theta_{\text{full}}}$ is the Jacobian w.r.t. Θ . Therefore,

$$\text{Var}(H^{(t)}) \approx J_{\Theta_{\text{full}}} \text{Var}(\Theta^{(t)}) J_{\Theta_{\text{full}}}^{\top} = \mathcal{O}\left(\frac{1}{t}\right). \quad (48)$$

Hence the variance of the embeddings also decays on the order of $1/t$.

VI. Final Conclusions

Expectation Consistency:

Every subgraph-based gradient is an unbiased estimator of the full-graph objective’s gradient. Therefore, $\Theta^{(t)}$ converges in expectation to Θ_{full} , and

$$\lim_{t \rightarrow \infty} \mathbb{E}[H^{(t)}] = H_{\text{full}}. \quad (49)$$

Variance Reduction:

With diminishing learning rates, $\text{Var}(\Theta^{(t)})$ remains bounded and often scales like $\mathcal{O}(1/t)$. Consequently,

$$\text{Var}(H^{(t)}) = \mathcal{O}\left(\frac{1}{t}\right). \quad (50)$$

Thus, the final embeddings increasingly concentrate around the full-graph GCN solution as t grows. *Summary.* After t subgraph samplings and training iterations, the final node embeddings’ expectation converges to the result of training a weighted GCN on the entire graph G . The variance of these embeddings decreases at a rate of $\mathcal{O}(1/t)$, ensuring they become more stable and closer to the full-graph solution as t increases. \square

D Limitations and Broader impacts

Limitations While SamGoG focuses on imbalanced graph classification task, the GoG technique is not limited to this specific task and can be extended to a broader range of graph learning applications, such as subgraph matching, link prediction, graph regression, and more. Additionally, as a specialized paradigm in graph learning, the efficiency of GoG still has room for improvement. Future research could focus on optimizing the framework to enhance its efficiency and applicability to larger and more complex datasets, thereby expanding its potential impact in diverse graph-based learning scenarios.

Broader Impacts SamGoG addresses imbalanced graph classification, offering improved detection accuracy for applications like identifying risk groups in social networks and recognizing protein properties.

E Additional Results on IGL-Bench

E.1 Performance of Class Imbalance Classification

Table 6: Accuracy (% \pm stddev) on datasets with changing class imbalance levels over 10 runs, encoded by GIN / GCN. **Red** and **Blue** highlight the best and second-best results respectively.

Algorithm	PTC-MR	D&D	IMDB-B	REDDIT-B
Balance ($\rho_{\text{class}} = 5 : 5$)				
GIN (bb.) [17]	50.43 \pm 2.69	64.04 \pm 3.79	66.05 \pm 2.57	76.66 \pm 4.80
G ² GNN [15]	53.70 \pm 3.87	66.07 \pm 2.27	61.91 \pm 3.77	72.34 \pm 2.76
TopoImb [8]	50.91 \pm 2.18	66.57 \pm 3.81	66.28 \pm 1.85	73.99 \pm 1.18
DataDec [35]	54.05 \pm 4.85	64.46 \pm 1.88	64.09 \pm 5.75	79.29\pm8.18
ImGKB [14]	53.48 \pm 3.50	65.45 \pm 2.88	50.16 \pm 0.34	50.24 \pm 0.29
SamGoG	59.71\pm2.12	72.59\pm1.93	69.27\pm1.53	77.74 \pm 0.50
Low Imbalance ($\rho_{\text{class}} = 7 : 3$)				
GIN (bb.) [17]	47.83 \pm 2.95	51.05 \pm 5.07	62.31 \pm 3.99	61.10 \pm 4.86
G ² GNN [15]	51.88 \pm 6.23	56.29 \pm 7.30	63.87 \pm 4.64	69.58 \pm 3.59
TopoImb [8]	44.86 \pm 3.52	49.97 \pm 7.24	59.95 \pm 5.19	59.67 \pm 7.30
DataDec [35]	55.72 \pm 2.88	63.51 \pm 1.62	67.92 \pm 3.37	78.39 \pm 5.01
ImGKB [14]	50.11 \pm 5.95	65.85 \pm 3.70	47.74 \pm 0.29	48.57 \pm 2.14
SamGoG	57.25\pm2.85	73.31\pm1.99	67.96\pm0.57	78.67\pm1.44
High Imbalance ($\rho_{\text{class}} = 9 : 1$)				
GIN (bb.) [17]	39.42 \pm 1.87	41.54 \pm 6.57	53.57 \pm 3.21	55.56 \pm 7.85
G ² GNN [15]	46.52 \pm 9.94	55.38 \pm 15.60	59.44 \pm 6.49	63.22 \pm 4.67
TopoImb [8]	39.42 \pm 1.24	39.12 \pm 1.62	47.75 \pm 3.73	51.58 \pm 4.69
DataDec [35]	58.69 \pm 3.10	65.77 \pm 2.71	66.30 \pm 6.70	77.72 \pm 5.12
ImGKB [14]	44.24 \pm 5.65	59.99 \pm 7.57	47.08 \pm 3.72	51.25 \pm 5.10
SamGoG	58.81\pm2.30	71.94\pm1.73	66.66\pm2.25	78.41\pm1.63

Table 7: **Balanced Accuracy** ($\% \pm \text{stddev}$) on datasets with changing class imbalance levels over 10 runs, encoded by GIN / GCN. **Red** and **Blue** highlight the best and second-best results respectively.

Algorithm	PTC-MR	D&D	IMDB-B	REDDIT-B
Balance ($\rho_{\text{class}} = 5 : 5$)				
GIN (bb.) [17]	51.40 \pm 1.64	63.37 \pm 3.26	66.05 \pm 2.57	76.66 \pm 4.80
G ² GNN [15]	53.42 \pm 3.72	63.79 \pm 2.13	61.91 \pm 3.77	72.34 \pm 2.76
TopoImb [8]	53.99 \pm 2.19	67.19 \pm 2.46	66.28 \pm 1.85	73.99 \pm 1.18
DataDec [35]	53.70 \pm 4.25	62.96 \pm 1.21	64.22 \pm 5.73	79.80\pm7.38
ImGKB [14]	53.34 \pm 3.61	62.33 \pm 4.38	49.99 \pm 0.47	50.24 \pm 0.29
SamGoG	57.19\pm3.33	73.45\pm1.07	69.28\pm1.53	77.74 \pm 0.50
Low Imbalance ($\rho_{\text{class}} = 7 : 3$)				
GIN (bb.) [17]	51.36 \pm 2.25	57.33 \pm 3.16	63.54 \pm 3.46	62.89 \pm 4.61
G ² GNN [15]	52.75 \pm 2.14	61.09 \pm 4.11	64.28 \pm 5.02	70.26 \pm 3.41
TopoImb [8]	50.44 \pm 3.75	58.33 \pm 4.40	61.14 \pm 4.56	61.34 \pm 6.80
DataDec [35]	53.42 \pm 2.33	61.27 \pm 1.04	67.95 \pm 2.77	78.68 \pm 4.93
ImGKB [14]	51.61 \pm 3.12	63.39 \pm 1.76	50.23 \pm 0.28	50.07 \pm 0.15
SamGoG	54.03\pm1.21	73.39\pm1.50	68.02\pm0.49	78.85\pm1.42
High Imbalance ($\rho_{\text{class}} = 9 : 1$)				
GIN (bb.) [17]	47.89 \pm 2.12	52.47 \pm 4.58	57.46 \pm 2.77	59.54 \pm 7.11
G ² GNN [15]	50.76 \pm 1.78	53.17 \pm 2.90	61.85 \pm 5.36	65.97 \pm 4.07
TopoImb [8]	49.99 \pm 0.93	52.05 \pm 1.31	52.82 \pm 3.06	55.87 \pm 4.09
DataDec [35]	55.22 \pm 3.81	61.60 \pm 2.60	66.30 \pm 4.93	77.77 \pm 5.49
ImGKB [14]	51.38 \pm 3.53	59.14 \pm 4.10	50.07 \pm 0.35	50.28 \pm 0.23
SamGoG	55.80\pm3.58	69.60\pm2.24	67.40\pm2.04	78.74\pm1.33

Table 8: **Macro-F1** ($\% \pm \text{stddev}$) on datasets with changing class imbalance levels over 10 runs, encoded by GIN / GCN. **Red** and **Blue** highlight the best and second-best results respectively.

Algorithm	PTC-MR	D&D	IMDB-B	REDDIT-B
Balance ($\rho_{\text{class}} = 5 : 5$)				
GIN (bb.) [17]	48.85 \pm 3.33	59.87 \pm 7.24	65.24 \pm 3.21	76.20 \pm 5.00
G ² GNN [15]	52.88 \pm 3.70	63.31 \pm 2.42	60.99 \pm 3.50	71.74 \pm 3.14
TopoImb [8]	48.33 \pm 3.70	65.72 \pm 3.45	65.85 \pm 2.29	73.41 \pm 0.01
DataDec [35]	52.98 \pm 4.65	62.83 \pm 1.20	62.42 \pm 8.07	79.02\pm8.63
ImGKB [14]	50.36 \pm 5.89	61.06 \pm 7.96	35.27 \pm 4.74	33.97 \pm 0.42
SamGoG	56.03\pm4.56	72.08\pm1.63	69.04\pm1.57	77.72 \pm 0.52
Low Imbalance ($\rho_{\text{class}} = 7 : 3$)				
GIN (bb.) [17]	46.63 \pm 2.95	49.89 \pm 6.19	59.66 \pm 5.94	56.10 \pm 6.75
G ² GNN [15]	47.64 \pm 7.63	55.34 \pm 8.20	61.37 \pm 8.64	69.03 \pm 3.78
TopoImb [8]	40.26 \pm 2.06	47.37 \pm 9.53	56.78 \pm 8.24	54.07 \pm 11.22
DataDec [35]	52.31 \pm 3.50	61.12 \pm 1.22	67.42 \pm 3.69	77.96 \pm 5.66
ImGKB [14]	44.62 \pm 8.86	62.91 \pm 2.34	32.70 \pm 0.62	32.81 \pm 1.21
SamGoG	52.95\pm1.71	72.28\pm1.74	67.78\pm0.65	78.66\pm1.44
High Imbalance ($\rho_{\text{class}} = 9 : 1$)				
GIN (bb.) [17]	35.14 \pm 4.01	38.83 \pm 8.36	47.51 \pm 5.47	48.74 \pm 11.66
G ² GNN [15]	37.35 \pm 7.10	42.22 \pm 11.10	56.79 \pm 9.27	61.15 \pm 6.30
TopoImb [8]	32.16 \pm 3.27	34.24 \pm 2.40	36.64 \pm 6.35	41.81 \pm 9.90
DataDec [35]	54.76 \pm 4.61	61.67 \pm 2.67	64.82 \pm 8.14	77.39 \pm 5.38
ImGKB [14]	41.35 \pm 7.92	57.16 \pm 5.54	32.23 \pm 1.61	34.31 \pm 2.68
SamGoG	55.24\pm3.44	69.20\pm1.92	66.63\pm2.26	78.36\pm1.58

Table 9: **Accuracy** ($\% \pm \text{stddev}$) on datasets with changing class imbalance levels over 10 runs, encoded by GIN / GCN. **Red** and **Blue** highlight the best and second-best results respectively.

Algorithm	PTC-MR	D&D	IMDB-B	REDDIT-B
Balance ($\rho_{\text{class}} = 5 : 5$)				
GCN (bb.) [4]	48.62 \pm 7.12	63.97 \pm 4.09	59.76 \pm 1.78	66.65 \pm 1.06
G ² GNN [15]	44.35 \pm 4.32	61.47 \pm 7.70	58.35 \pm 3.47	67.02 \pm 2.55
TopoImb [8]	50.61 \pm 6.39	56.13 \pm 4.61	49.52 \pm 1.01	58.62 \pm 6.52
DataDec [35]	54.23 \pm 4.16	63.10 \pm 2.62	58.20 \pm 4.05	69.08 \pm 4.49
ImGKB [14]	52.83 \pm 5.45	64.93 \pm 4.44	50.15 \pm 0.39	50.29 \pm 0.19
SamGoG	59.49 \pm 2.68	75.13 \pm 0.90	71.70 \pm 0.79	80.05 \pm 0.23
Low Imbalance ($\rho_{\text{class}} = 7 : 3$)				
GCN (bb.) [4]	43.84 \pm 7.03	58.32 \pm 1.51	49.06 \pm 2.17	61.85 \pm 3.89
G ² GNN [15]	47.86 \pm 9.03	65.65 \pm 5.41	53.11 \pm 3.97	66.02 \pm 2.08
TopoImb [8]	45.90 \pm 6.41	44.63 \pm 4.82	49.75 \pm 4.81	54.35 \pm 3.13
DataDec [35]	55.86 \pm 2.49	64.66 \pm 2.04	57.06 \pm 5.97	66.45 \pm 5.38
ImGKB [14]	49.49 \pm 5.12	67.44 \pm 3.50	47.65 \pm 0.23	48.58 \pm 2.15
SamGoG	56.98 \pm 3.65	74.81 \pm 0.99	68.35 \pm 1.59	80.03 \pm 1.03
High Imbalance ($\rho_{\text{class}} = 9 : 1$)				
GCN (bb.) [4]	40.58 \pm 7.61	42.48 \pm 2.61	45.09 \pm 0.18	54.39 \pm 5.16
G ² GNN [15]	41.78 \pm 7.61	44.59 \pm 4.72	56.40 \pm 1.71	65.08 \pm 3.08
TopoImb [8]	40.17 \pm 2.21	36.50 \pm 1.44	46.18 \pm 3.06	52.21 \pm 3.56
DataDec [35]	55.41 \pm 3.37	65.07 \pm 2.40	58.58 \pm 5.07	65.56 \pm 8.61
ImGKB [14]	45.98 \pm 8.71	58.21 \pm 10.60	46.06 \pm 2.74	51.23 \pm 5.09
SamGoG	59.49 \pm 1.26	66.90 \pm 1.83	61.55 \pm 1.30	76.71 \pm 1.30

Table 10: **Balanced Accuracy** ($\% \pm \text{stddev}$) on datasets with changing class imbalance levels over 10 runs, encoded by GIN / GCN. **Red** and **Blue** highlight the best and second-best results respectively.

Algorithm	PTC-MR	D&D	IMDB-B	REDDIT-B
Balance ($\rho_{\text{class}} = 5 : 5$)				
GCN (bb.) [4]	50.07 \pm 0.23	62.63 \pm 2.06	59.76 \pm 1.78	66.65 \pm 1.06
G ² GNN [15]	50.02 \pm 0.06	60.38 \pm 5.83	58.35 \pm 3.47	67.02 \pm 2.55
TopoImb [8]	53.71 \pm 2.88	60.56 \pm 2.30	49.71 \pm 0.34	58.68 \pm 6.48
DataDec [35]	54.36 \pm 3.61	61.41 \pm 2.42	58.11 \pm 3.96	69.08 \pm 4.38
ImGKB [14]	53.03 \pm 3.56	62.84 \pm 2.56	50.15 \pm 0.39	50.29 \pm 0.19
SamGoG	56.98\pm2.08	73.57\pm0.58	71.70\pm0.79	80.05\pm0.23
Low Imbalance ($\rho_{\text{class}} = 7 : 3$)				
GCN (bb.) [4]	49.69 \pm 0.68	60.53 \pm 1.43	51.35 \pm 1.88	63.51 \pm 3.57
G ² GNN [15]	49.73 \pm 0.87	65.61 \pm 2.52	53.84 \pm 3.33	66.54 \pm 2.09
TopoImb [8]	51.60 \pm 3.14	54.87 \pm 2.95	48.94 \pm 4.07	56.51 \pm 2.84
DataDec [35]	54.50 \pm 1.74	62.01 \pm 1.75	56.87 \pm 5.73	67.02 \pm 5.12
ImGKB [14]	51.70 \pm 2.33	63.70 \pm 3.66	50.14 \pm 0.22	50.08 \pm 0.16
SamGoG	54.92\pm0.98	73.67\pm0.50	68.47\pm1.54	80.32\pm0.89
High Imbalance ($\rho_{\text{class}} = 9 : 1$)				
GCN (bb.) [4]	50.36 \pm 1.14	53.22 \pm 2.13	50.08 \pm 0.16	58.47 \pm 4.64
G ² GNN [15]	49.94 \pm 1.47	54.99 \pm 3.11	58.87 \pm 1.18	65.09 \pm 3.02
TopoImb [8]	50.78 \pm 0.68	49.47 \pm 1.20	51.02 \pm 2.25	56.40 \pm 2.67
DataDec [35]	53.28 \pm 2.65	60.83 \pm 2.61	58.11 \pm 4.26	66.61 \pm 6.89
ImGKB [14]	50.19 \pm 3.07	60.22 \pm 4.56	50.06 \pm 0.31	50.26 \pm 0.22
SamGoG	56.72\pm1.94	61.97\pm3.44	62.36\pm1.38	77.41\pm1.22

Table 11: **Macro-F1** ($\% \pm \text{stddev}$) on datasets with changing class imbalance levels over 10 runs, encoded by GIN / GCN. **Red** and **Blue** highlight the best and second-best results respectively.

Algorithm	PTC-MR	D&D	IMDB-B	REDDIT-B
Balance ($\rho_{\text{class}} = 5 : 5$)				
GCN (bb.) [4]	32.82 \pm 3.29	62.02 \pm 2.84	59.32 \pm 2.48	67.58 \pm 1.06
G ² GNN [15]	31.29 \pm 2.68	56.99 \pm 10.85	56.41 \pm 7.64	65.63 \pm 3.26
TopoImb [8]	45.01 \pm 8.36	55.05 \pm 4.87	33.04 \pm 0.43	50.17 \pm 12.11
DataDec [35]	53.24 \pm 3.23	61.35 \pm 2.55	54.26 \pm 7.60	67.37 \pm 6.20
ImGKB [14]	48.53 \pm 8.31	62.34 \pm 3.64	33.84 \pm 0.60	33.97 \pm 0.41
SamGoG	55.89\pm3.20	73.72\pm0.68	71.69\pm0.79	79.95\pm0.19
Low Imbalance ($\rho_{\text{class}} = 7 : 3$)				
GCN (bb.) [4]	31.49 \pm 5.35	58.06 \pm 1.46	36.70 \pm 6.23	57.56 \pm 6.17
G ² GNN [15]	33.06 \pm 4.46	64.18 \pm 4.21	45.81 \pm 10.04	65.51 \pm 2.39
TopoImb [8]	39.66 \pm 9.73	40.50 \pm 7.73	37.79 \pm 5.88	45.50 \pm 5.89
DataDec [35]	54.16\pm1.97	61.94 \pm 1.91	50.18 \pm 11.79	64.62 \pm 6.82
ImGKB [14]	45.80 \pm 7.16	63.41 \pm 4.10	32.52 \pm 0.48	32.82 \pm 1.24
SamGoG	53.80 \pm 0.87	73.27\pm0.63	68.25\pm1.59	79.99\pm1.05
High Imbalance ($\rho_{\text{class}} = 9 : 1$)				
GCN (bb.) [4]	29.74 \pm 6.39	40.59 \pm 3.18	31.21 \pm 0.36	47.46 \pm 8.81
G ² GNN [15]	32.13 \pm 7.08	42.79 \pm 6.25	54.41 \pm 2.63	64.77 \pm 3.25
TopoImb [8]	32.03 \pm 3.31	31.98 \pm 1.84	33.79 \pm 6.25	44.46 \pm 6.18
DataDec [35]	52.48 \pm 3.00	60.89 \pm 2.60	53.87 \pm 8.76	62.46 \pm 11.54
ImGKB [14]	39.08 \pm 8.03	55.46 \pm 11.43	31.73 \pm 0.22	34.27 \pm 2.64
SamGoG	56.32\pm1.80	61.77\pm3.86	61.44\pm1.29	76.68\pm1.31

E.2 Performance of Graph Size Imbalance Classification

Table 12: **Accuracy** (% \pm stddev) on datasets with changing size imbalance levels over 10 runs, encoded by GIN / GCN. **Red** and **Blue** highlight the best and second-best results respectively.

Algorithm	PTC-MR	D&D	IMDB-B	REDDIT-B
Low level ρ_{size}	1.60	1.56	1.64	2.79
GIN (bb.) [17]	52.17 \pm 4.36	65.01 \pm 0.69	66.38 \pm 4.27	67.41 \pm 2.32
SOLT-GNN [9]	47.54 \pm 4.33	63.78 \pm 1.06	64.20 \pm 5.46	49.57 \pm 6.78
TopoImb [8]	49.71 \pm 1.98	65.16 \pm 1.76	66.00 \pm 2.41	69.47 \pm 3.70
SamGoG	53.86\pm2.12	68.22\pm2.40	66.82\pm0.85	72.20\pm4.24
Mid level ρ_{size}	2.90	2.53	2.11	4.92
GIN (bb.) [17]	51.38 \pm 6.78	61.46 \pm 2.43	65.08 \pm 5.78	68.32 \pm 1.77
SOLT-GNN [9]	53.04 \pm 3.91	63.33 \pm 1.86	69.38 \pm 1.23	73.51 \pm 1.14
TopoImb [8]	51.59 \pm 4.30	65.99 \pm 1.25	68.10 \pm 0.87	71.54 \pm 0.75
SamGoG	57.17\pm1.06	71.91\pm1.22	69.53\pm1.01	79.12\pm0.90
High level ρ_{size}	4.93	8.91	4.45	10.97
GIN (bb.) [17]	48.41 \pm 7.07	60.68 \pm 6.89	62.60 \pm 3.82	67.41 \pm 2.23
SOLT-GNN [9]	51.74 \pm 5.25	64.97 \pm 3.24	65.03 \pm 4.12	60.24 \pm 2.11
TopoImb [8]	51.96 \pm 1.16	64.16 \pm 2.96	66.75 \pm 0.91	69.14 \pm 4.83
SamGoG	59.13\pm1.32	69.15\pm1.87	67.13\pm1.59	72.31\pm2.07

Table 13: **Balanced Accuracy** (% \pm stddev) on datasets with changing size imbalance levels over 10 runs, encoded by GIN / GCN. **Red** and **Blue** highlight the best and second-best results respectively.

Algorithm	PTC-MR	D&D	IMDB-B	REDDIT-B
Low level ρ_{size}	1.60	1.56	1.64	2.79
GIN (bb.) [17]	51.08 \pm 2.07	63.46 \pm 0.92	66.38 \pm 4.27	67.41 \pm 2.32
SOLT-GNN [9]	45.47 \pm 2.10	62.58 \pm 0.61	64.20 \pm 5.46	49.57 \pm 6.78
TopoImb [8]	50.07 \pm 2.77	67.24 \pm 1.53	66.00 \pm 2.41	69.47 \pm 3.70
SamGoG	52.66\pm2.33	71.20\pm1.78	66.82\pm0.85	72.20\pm4.24
Mid level ρ_{size}	2.90	2.53	2.11	4.92
GIN (bb.) [17]	49.83 \pm 1.30	62.22 \pm 0.98	65.08 \pm 5.78	68.32 \pm 1.77
SOLT-GNN [9]	50.06 \pm 0.75	59.61 \pm 3.40	69.38 \pm 1.23	73.51 \pm 1.14
TopoImb [8]	50.88 \pm 2.36	65.25 \pm 2.43	68.10 \pm 0.87	71.54 \pm 0.75
SamGoG	56.72\pm1.26	72.28\pm1.41	69.52\pm1.01	79.12\pm0.90
High level ρ_{size}	4.93	8.91	4.45	10.97
GIN (bb.) [17]	50.20 \pm 0.69	61.43 \pm 2.36	62.60 \pm 3.82	67.41 \pm 2.23
SOLT-GNN [9]	48.02 \pm 1.77	60.75 \pm 6.03	65.03 \pm 4.12	60.24 \pm 2.11
TopoImb [8]	52.07 \pm 0.96	66.48 \pm 1.89	66.75 \pm 0.91	69.14 \pm 4.83
SamGoG	56.92\pm1.62	68.48\pm1.19	67.13\pm1.59	72.31\pm2.07

Table 14: **Macro-F1** ($\% \pm \text{stddev}$) on datasets with changing size imbalance levels over 10 runs, encoded by GIN / GCN. **Red** and **Blue** highlight the best and second-best results respectively.

Algorithm	PTC-MR	D&D	IMDB-B	REDDIT-B
Low level ρ_{size}	1.60	1.56	1.64	2.79
GIN (bb.) [17]	48.26 \pm 3.11	63.39 \pm 0.84	65.67 \pm 5.40	66.14 \pm 1.90
SOLT-GNN [9]	43.63 \pm 1.91	62.34 \pm 0.66	63.66 \pm 5.94	49.17 \pm 6.76
TopoImb [8]	48.87 \pm 2.90	64.97 \pm 1.65	65.71 \pm 2.62	69.15 \pm 3.83
SamGoG	52.52\pm2.28	68.11\pm2.41	66.20\pm1.16	70.50\pm5.03
Mid level ρ_{size}	2.90	2.53	2.11	4.92
GIN (bb.) [17]	38.58 \pm 5.97	60.89 \pm 1.84	63.28 \pm 9.06	67.20 \pm 2.32
SOLT-GNN [9]	43.20 \pm 5.36	58.67 \pm 4.91	68.73 \pm 1.97	73.24 \pm 1.40
TopoImb [8]	49.17 \pm 0.95	64.65 \pm 1.76	67.98 \pm 0.95	71.52 \pm 0.75
SamGoG	56.39\pm1.19	71.34\pm1.28	69.45\pm0.98	79.10\pm0.90
High level ρ_{size}	4.93	8.91	4.45	10.97
GIN (bb.) [17]	34.56 \pm 6.32	57.98 \pm 5.51	59.75 \pm 6.69	66.20 \pm 2.77
SOLT-GNN [9]	40.70 \pm 3.27	58.50 \pm 10.48	64.53 \pm 4.68	54.80 \pm 3.23
TopoImb [8]	51.65 \pm 1.07	63.97 \pm 2.78	66.67 \pm 0.91	68.41 \pm 5.34
SamGoG	56.44\pm1.73	68.08\pm1.53	67.13\pm1.59	71.92\pm2.13

Table 15: **Accuracy** ($\% \pm \text{stddev}$) on datasets with changing size imbalance levels over 10 runs, encoded by GIN / GCN. **Red** and **Blue** highlight the best and second-best results respectively.

Algorithm	PTC-MR	D&D	IMDB-B	REDDIT-B
Low level ρ_{size}	1.60	1.56	1.64	2.79
GCN (bb.) [4]	51.59 \pm 7.07	64.82 \pm 0.75	69.15 \pm 1.44	53.44 \pm 1.78
SOLT-GNN [9]	51.45 \pm 3.13	65.69 \pm 2.36	68.23 \pm 2.48	37.58 \pm 3.04
TopoImb [8]	46.74 \pm 1.57	56.18 \pm 2.10	68.20 \pm 0.70	56.94 \pm 3.23
SamGoG	52.83\pm0.90	71.06\pm3.54	70.53\pm0.87	72.60\pm1.72
Mid level ρ_{size}	2.90	2.53	2.11	4.92
GCN (bb.) [4]	50.00 \pm 5.87	63.99 \pm 2.16	67.95 \pm 2.82	67.96 \pm 0.89
SOLT-GNN [9]	56.23 \pm 0.84	62.78 \pm 1.33	70.25 \pm 1.15	61.95 \pm 5.55
TopoImb [8]	54.13 \pm 4.62	64.73 \pm 7.09	68.75 \pm 0.76	69.12 \pm 0.52
SamGoG	57.03\pm1.46	72.80\pm2.53	70.54\pm0.40	79.08\pm1.36
High level ρ_{size}	4.93	8.91	4.45	10.97
GCN (bb.) [4]	49.93 \pm 5.90	60.98 \pm 6.71	64.88 \pm 2.02	66.38 \pm 0.46
SOLT-GNN [9]	54.78 \pm 6.03	63.21 \pm 3.40	69.80\pm2.07	67.05 \pm 2.54
TopoImb [8]	51.81 \pm 1.26	69.66 \pm 1.92	66.60 \pm 0.91	69.09 \pm 1.00
SamGoG	59.71\pm1.46	74.65\pm1.45	69.38 \pm 0.30	77.29\pm1.26

Table 16: **Balanced Accuracy** ($\% \pm \text{stddev}$) on datasets with changing size imbalance levels over 10 runs, encoded by GIN / GCN. **Red** and **Blue** highlight the best and second-best results respectively.

Algorithm	PTC-MR	D&D	IMDB-B	REDDIT-B
Low level ρ_{size}	1.60	1.56	1.64	2.79
GCN (bb.) [4]	50.47 \pm 0.75	63.13 \pm 0.43	69.15 \pm 1.44	53.44 \pm 1.78
SOLT-GNN [9]	48.24 \pm 1.20	63.81 \pm 1.86	68.23 \pm 2.48	37.58 \pm 3.04
TopoImb [8]	50.43 \pm 0.87	57.64 \pm 0.94	68.20 \pm 0.70	56.94 \pm 3.23
SamGoG	53.33\pm0.27	70.46\pm3.84	70.52\pm0.87	72.60\pm1.72
Mid level ρ_{size}	2.90	2.53	2.11	4.92
GCN (bb.) [4]	49.74 \pm 2.52	58.27 \pm 4.65	67.95 \pm 2.82	67.96 \pm 0.89
SOLT-GNN [9]	51.13 \pm 0.79	59.12 \pm 2.47	70.25 \pm 1.15	61.95 \pm 5.55
TopoImb [8]	54.34 \pm 3.22	64.63 \pm 3.42	68.75 \pm 0.76	69.12 \pm 0.52
SamGoG	55.99\pm1.54	70.50\pm1.79	70.54\pm0.40	79.08\pm1.36
High level ρ_{size}	4.93	8.91	4.45	10.97
GCN (bb.) [4]	49.96 \pm 0.54	57.58 \pm 4.32	64.88 \pm 2.02	66.38 \pm 0.46
SOLT-GNN [9]	51.11 \pm 1.15	60.94 \pm 1.68	69.80\pm2.07	67.05 \pm 2.54
TopoImb [8]	52.12 \pm 0.78	66.63 \pm 4.54	66.60 \pm 0.91	69.09 \pm 1.00
SamGoG	58.05\pm1.26	72.39\pm1.91	69.38 \pm 0.30	77.29\pm1.26

Table 17: **Macro-F1** ($\% \pm \text{stddev}$) on datasets with changing size imbalance levels over 10 runs, encoded by GIN / GCN. **Red** and **Blue** highlight the best and second-best results respectively.

Algorithm	PTC-MR	D&D	IMDB-B	REDDIT-B
Low level ρ_{size}	1.60	1.56	1.64	2.79
GCN (bb.) [4]	36.72 \pm 5.58	63.09 \pm 0.46	69.02 \pm 1.52	49.68 \pm 8.19
SOLT-GNN [9]	45.00 \pm 3.14	63.82 \pm 2.01	67.88 \pm 2.35	35.00 \pm 2.77
TopoImb [8]	44.72 \pm 2.61	55.77 \pm 1.91	67.78 \pm 1.00	56.09 \pm 3.68
SamGoG	52.51\pm0.51	70.02\pm3.71	70.45\pm0.84	71.77\pm2.05
Mid level ρ_{size}	2.90	2.53	2.11	4.92
GCN (bb.) [4]	40.94 \pm 5.67	54.22 \pm 8.96	67.80 \pm 2.84	67.18 \pm 1.39
SOLT-GNN [9]	45.63 \pm 4.84	58.14 \pm 3.23	70.05 \pm 1.19	57.57 \pm 8.59
TopoImb [8]	51.99 \pm 3.88	62.10 \pm 6.59	68.64 \pm 0.77	69.10 \pm 0.49
SamGoG	55.67\pm1.75	70.83\pm2.10	70.54\pm0.41	79.05\pm1.38
High level ρ_{size}	4.93	8.91	4.45	10.97
GCN (bb.) [4]	39.32 \pm 7.82	52.46 \pm 8.79	63.65 \pm 3.15	65.91 \pm 0.31
SOLT-GNN [9]	39.57 \pm 6.16	60.32 \pm 2.31	69.54\pm2.16	65.40 \pm 3.77
TopoImb [8]	51.43 \pm 0.98	65.66 \pm 5.28	66.54 \pm 0.89	68.76 \pm 1.17
SamGoG	58.00\pm1.30	72.73\pm1.85	69.35 \pm 0.32	77.24\pm1.27

E.3 Performance on Different Downstream Models

Table 18: **Accuracy** score ($\% \pm \text{stddev}$) on **D&D** dataset with different class imbalance levels over 10 runs. **Red** and **Blue** highlight the best and second-best results respectively.

Algorithm	Balance	Low Imbalance	High Imbalance
ρ_{class}	1:1	7:3	9:1
GIN (bb.) [17]	64.04 \pm 3.79	51.05 \pm 5.07	41.54 \pm 6.57
G ² GNN [15]	66.07 \pm 2.27	56.29 \pm 7.30	55.38 \pm 15.60
TopoImb [8]	66.57 \pm 3.81	49.97 \pm 7.24	39.12 \pm 1.62
DataDec [35]	64.46 \pm 1.88	63.51 \pm 1.62	65.77 \pm 2.71
ImGKB [14]	65.45 \pm 2.88	65.85 \pm 3.70	59.99 \pm 7.57
SamGoG (w/ TailGNN [31])	72.59\pm1.93	73.31 \pm 1.99	71.94\pm1.73
SamGoG (w/ GraphSHA [40])	71.73 \pm 2.53	73.99\pm0.98	70.35 \pm 1.62

Table 19: **Accuracy** score ($\% \pm \text{stddev}$) on **D&D** dataset with different class imbalance levels over 10 runs. **Red** and **Blue** highlight the best and second-best results respectively.

Algorithm	Balance	Low Imbalance	High Imbalance
ρ_{class}	1:1	7:3	9:1
GCN (bb.) [4]	63.97 \pm 4.09	58.32 \pm 1.51	42.48 \pm 2.61
G ² GNN [15]	61.47 \pm 7.70	65.65 \pm 5.41	44.59 \pm 4.72
TopoImb [8]	56.13 \pm 4.61	44.63 \pm 4.82	36.50 \pm 1.44
DataDec [35]	63.10 \pm 2.62	64.66 \pm 2.04	65.07 \pm 2.40
ImGKB [14]	64.93 \pm 4.44	67.44 \pm 3.50	58.21 \pm 10.60
SamGoG (w/ TailGNN [31])	75.13\pm0.90	74.81 \pm 0.99	66.90 \pm 1.83
SamGoG (w/ GraphSHA [40])	73.91 \pm 1.65	74.94\pm1.85	70.07\pm2.94

Table 20: **Accuracy** score ($\% \pm \text{stddev}$) on **D&D** dataset with different graph size imbalance levels over 10 runs. **Red** and **Blue** highlight the best and second-best results respectively.

Algorithm	Balance	Low Imbalance	High Imbalance
ρ_{size}	1.56	2.53	8,91
GIN (bb.) [17]	65.01 \pm 0.69	61.46 \pm 2.43	60.68 \pm 6.89
SOLT-GNN [9]	63.78 \pm 1.06	63.33 \pm 1.86	64.97 \pm 3.24
TopoImb [8]	65.16 \pm 1.76	65.99 \pm 1.25	64.16 \pm 2.96
SamGoG (w/ TailGNN [31])	68.22\pm2.40	71.91\pm1.22	69.15 \pm 1.87
SamGoG (w/ GraphSHA [40])	66.71 \pm 2.07	71.17 \pm 1.53	70.00\pm1.83

Table 21: **Accuracy** score ($\% \pm \text{stddev}$) on **D&D** dataset with different graph size imbalance levels over 10 runs. **Red** and **Blue** highlight the best and second-best results respectively.

Algorithm	Balance	Low Imbalance	High Imbalance
ρ_{size}	1.56	2.53	8,91
GCN (bb.) [4]	64.82 \pm 0.75	63.99 \pm 2.16	60.98 \pm 6.71
SOLT-GNN [9]	65.69 \pm 2.36	62.78 \pm 1.33	63.21 \pm 3.40
TopoImb [8]	56.18 \pm 2.10	64.73 \pm 7.09	69.66 \pm 1.92
SamGoG (w/ TailGNN [31])	71.06\pm3.54	72.80\pm2.53	74.65\pm1.45
SamGoG (w/ GraphSHA [40])	68.54 \pm 1.72	72.21 \pm 2.79	71.98 \pm 2.06